Definition of seismic performances and fragility curves of unanchored cylindrical steel legged tanks used in wine making and storage

Definition of seismic performances and fragility curves of unanchored cylindrical steel legged tanks used in wine making and storage

M. Bovo*, A. Barbaresi, D. Torreggiani

DISTAL Department, Engineering Agriculture – University of Bologna
Viale G. Fanin, 48 - 40127 Bologna, Italy
* Corresponding author. E-mail: marco.bovo@unibo.it

ABSTRACT

The introduction of stainless-steel legged tanks is rather recent, and their use increased in the last decades in exponential way, especially in food industry and agricultural applications since they proved to be simple to prefabricate and transport, easy to clean and chemically inert. Despite their worldwide diffusion also in high seismicity areas, most of them were not designed with earthquake-based criteria as emerged by the catastrophic consequences and heavy losses observed, even recently, after several major earthquakes.

By means of incremental dynamic analyses on the finite element models of 140 winemaking and storage legged tanks, the present paper, evaluates the main features of the dynamic response and for each vessel provides the lognormal cumulative fragility functions, for three different limit states of each vessel. Then, for each limit state, by means of nonlinear regression analyses, the median and the dispersion parameters of the best fitting lognormal function of every tank were statistically elaborated in order to define the response surfaces of the parameters.

The response surfaces, provided for 3-, 4- and 5-leg unanchored tanks, are defined on the basis of few geometrical tank data. The analytical expressions provided in the paper, represent a practical and useful tool to directly calculate the fragilities of legged vessel. These, obviously, will allow the fast assessment of the seismic vulnerability of the tanks in agricultural facilities located in seismic prone areas.

Keywords: wine storage; legged tank; seismic performance; fragility curve; response surface.

1. INTRODUCTION

The introduction of stainless-steel tanks in civil engineering applications is rather recent and their use increased in exponential way in the last decades. Nowadays, they are used for several applications to store liquids (e.g. water, wine, oil, nitrogen, petroleum) and high-pressure gas as well. Furthermore, the steel tanks result relatively simple to prefabricate and transport, easy to clean, chemically inert so to become very common in food industry and agricultural facilities to safely contain edible products. In order to minimize the material quantity, these vessels had thickness-optimised elements and, in general, were mainly designed against the content-induced loads (i.e. internal pressure of liquid or gas) and the most of them were not designed with earthquake-based criteria (Cooper 2004). Consequently, several major earthquakes in the world affected these tanks producing catastrophic consequences and inducing heavy losses (Swan et al. 1984; Manos 1991; Brunesi et al. 2014).

Following the consolidated literature approach, the cylindrical steel tanks are classified in two main categories: the flat-base (or continuously supported) tanks and the leg-supported (or legged) tanks (Gonzalez et al. 2013). Moreover, based on their use, the vessels usually adopted in the wine making and storage process are subdivided in fermenters, used during production phase and conservation of red wine, and storage tanks adopted to store large wine quantities. Typically, the fermenters are legged whereas the storage tanks can be both legged and flat-base, with the latter able to hold several hectolitres of wine. As stated before, steel vessels result very sensitive to earthquake excitation, as confirmed by the copious damage reports emerged in the aftermath of past worldwide seismic events (e.g. 1977 Caucete Earthquake (Manos 1991), 1980 Greenville Earthquake (Niwa and Clough 1982), 1984 Morgan Hill Earthquake (Swan et al. 1984), 1989 Loma Prieta Earthquake (EERI 1990), 2003 San Simeon Earthquake (EERI 2004), 2007 Pisco Earthquake (Taucer et al. 2008), 2007 Maule Earthquake (Gonzalez et al. 2013), 2012 Emilia Earthquake (Brunesi et al. 2014),

Kaikoura earthquake (Dizhur et al. 2017)). The most common collapses produced by the past earthquakes in flat-base tanks were: failure of anchors, elephant's foot buckling close to the base of squat tanks, diamond-shaped buckling on the wall of slender tanks (Brunesi et al. 2014). Differently, with reference to the legged tanks, the base-anchor failure, shear failure or buckling of the legs, overturning and excessive sliding, were the most observed collapse and damage mechanisms. Therefore, the poor seismic response of this class of structures is evident and well-known. Moreover, it is to highlight that, as an unfortunately coincidence, a considerable quantity of the world wine production is located in countries with seismic prone areas (i.e. Italy, Spain, California, Chile, Argentina, South Africa, Portugal, New Zealand, Greece) with some of them characterized even by moderate-high seismic hazard.

Various studies have been carried out to investigate the dynamic response and the collapse mechanisms of existing flat-base vessels (Haroun and Housner 1982; Leon 1986; Haroun and Ellaithy 1985; Haroun and Tavel 1985), especially regarding liquid storage containers in industrial plants. On the contrary, very few works on the safety of steel legged tanks exist (Brunesi et al. 2014; Gonzalez et al. 2013). The current literature providing tank fragility functions is even poorer. Observational-based seismic fragility relations are provided in Salzano et al. (2003) whereas Berahman and Behnamfar (2007) proposed a Bayesian-based method for evaluate the seismic fragilities of unanchored steel tanks. Iervolino et al. (2004) proposed a rational procedure for the seismic vulnerability assessment of industrial tanks with fragility curves obtained by means of a response surface-based method. More recently, buckling tank fragility functions, obtained by means of Incremental Dynamic Analysis (IDA), were provided by Buratti and Tavano (2014). A comparison between cloud analysis and IDA was carried out by Phan et al. (2016) with the purpose of providing fragilities for two aboveground existing cylindrical steel tanks of an industrial plant and one elevated tank supported by reinforced concrete columns (Phan et al. 2017). Finally, the collapse fragilities of existing legged tanks are used in (Colombo and Almazan 2017; Auad and Almazan 2017)

for the validation of the retrofitting interventions adopting seismic isolation devices. Nowadays, it is well established that the evaluation of the seismic vulnerability of the existing vessels is an important matter and seismic fragility functions proved to be a powerful tool in order to quantify their seismic sensitivity.

In this field, the present paper firstly provides the seismic fragilities, for different limit state conditions, of a large stock of unanchored cylindrical steel legged tanks used in wine-making industry. The 140 vessels of the stock were classified in three different groups based on the number of supporting legs. The three groups, with respectively 20 three-leg, 110 four-leg and 10 five-leg vessels, are representative of a large percentage of the existing tanks currently adopted in Italy, but also in other countries around the world where wine is produced, aged and stored before the final sale. The numerical fragilities were obtained, for each tank, with IDA performed on three-dimensional finite element model (FEM) considering all the three ground-motion components (i.e. two horizontals and one vertical). It is worth to note that, for each tank model, incremental dynamic analyses have been performed considering different ground-motion entrance directions (labelled "configuration" in the following) in order to consider the radial asymmetry introduced, in the dynamic behaviour, by the presence of discrete supports (i.e. the legs).

Then, the numerical fragilities were fitted by lognormal cumulative distribution, so obtaining via maximum likelihood method the parameters of the distribution (i.e. e^{μ} and σ respectively median and dispersion) for each tank, for the three different limit states.

Finally, starting by the lognormal best fitting fragilities, an analytical expression for the response (fragility) surface of both e^{μ} and σ was then calibrated for each group (i.e. 3-, 4- and 5-leg). The response surfaces allow to define a relationship between the failure/damage probability, the seismic intensity measure and the structural characteristics most influencing the seismic response of the tanks investigated here.

Since the high standardization of legged stainless-steel tanks in the wine industry, the results of this paper can be considered as reference for several tanks in most countries of the world. The analytical expressions provided in the paper, represent a practical and useful tool for the direct evaluation of the fragilities of cylindrical steel legged vessels having similar characteristics to those investigated here.

2. DESCRIPTION AND NUMERICAL MODELLING OF THE STOCK

2.1 Main characteristics of cylindrical steel legged vessels

A stock of 140 cylindrical steel legged vessels was considered in the present study. The detailed data and the main characteristics of the most common typologies were extracted by the technical reports made available directly by the producers. The stock was created by selecting some of the most typical vessel types used in Europe and North America areas, since these areas host about 70% of the total worldwide wine production and storage (Italian Wine Central 2019).

In the paper, two legged vessel types were considered: tanks and fermenters. The formers are usually adopted for storage and long conservation, while the latter are typically adopted in the wine-production phase and sometimes for temporary conservation. The stock contains a total of 62 storage tanks and 78 fermenters with conical, plain or jacketed bottom. A general view, of the two vessel typologies considered in the study, is reported in Figure 1 (Petramale 2019). The main characteristics of the stock in terms of typology, geometrical dimensions and storage capacity were collected in Table 1 (see Appendix) adopting the same symbols in Figure 1. The stock was selected in order to cover a wide range of storage capacity C, i.e. from 0.3 m^3 to 100m^3 (with the assumption that 1 m^3 is equivalent to 1 kilolitre), different vessel total heights H, from 1.40m to 12.85m (with $H = H_{leg} + H_{wall}$ where: H_{leg} is the leg length and H_{wall} is the height of the mantle wall tank), and various aspect ratios $\lambda = H / D$ (where: D is the

outer diameter of the mantle wall). D ranges from 636mm to 3500mm. In Table 1 is reported the total mass (Mass) obtained considering both wine and vessel. Figure 2a represents, for each group (i.e. 3-, 4- and 5-leg), the distribution of λ vs. C. Instead, Figure 2b shows the distributions of the ratio H_{wall} / H_{leg} vs. C. λ will result useful in the following, since it is correlated to the center of mass elevation and will be also introduced in the analytical relation defining the response (fragility) surface. In the stock, λ goes from 1.0 to 4.28. It is to highlight that λ values of the vessels studied here are rather different from the typical values of tanks in the industrial facilities (typically storing larger fluid quantity and characterized by $\lambda < 1$) and, obviously, the two dynamic behaviours result very different. The thickness of mantle wall and roof goes from 1mm to 2mm, whereas it ranges from 1.5 to 3mm at the bottom, typically stiffened with a steel ring. The legs are cold formed squared or circular, tapered or constant, with main cross-sections dimension (d) around 200-300mm and thickness (t) of 2-3mm. The ratio d/t results larger than 100, and then, the legs cross-section can be considered slender (equivalent to a class 4) following the classification in the Eurocode 3 (CEN 2004). Therefore, for this cross-section, a fully plastic behaviour is not allowed since the local buckling instability deteriorates the section. The leg length varies from 300mm to 1050mm. The tanks in the stock are fabricated with stainless steel AISI 304L (ASTM 2018).

In the present paper, the tanks were considered unanchored to the floor, as usually occurs. This is an important fact since the anchoring systems play a fundamental role in the definition of the dynamic behaviour of the structure. The anchored tanks and the evaluation of their seismic vulnerability will be the subject of future investigations.

2.2 Description of seismic behaviour and typical damage mechanisms

The seismic behaviour of circular steel tanks containing liquids was investigated by many researchers usually obtaining the structural response by considering the effects of

hydrodynamic fluid–structure interaction (Hamdan 2000; Veletsos and Shivakumar 1997; Rammerstorfer et al. 1990; Veletsos 1984; Haroun and Housner 1981; Hunt and Priestley 1978; Veletsos and Yang 1977; Housner 1963; Jacobsen 1949). One of the most used approach to solve the problem, is to evaluate the whole hydrodynamic response of the tank-liquid system by the superposition of two different contributions: the sloshing motion and the impulsive motion. If the tank wall is rigid, the lower portion of the fluid mass moves in unison with the tank wall and this represents the impulsive mass. The liquid that moves with a long period at the top of the tank under the free surface (sloshing motion), represents the convective mass. The total liquid mass can be split into two fractions characterized by two different oscillating periods and these two components can be considered uncoupled, because they show significant differences in their natural periods (Veletsos and Shivakumar 1997). The sloshing motion of the convective mass is usually associated to long periods, and then, to low seismic spectral acceleration. If this is the case, convective component introduces a low contribution to the total hydrodynamic pressure on the tank walls and the global tank response could be achieved by considering only the impulsive component.

In the present paper, in order to evaluate the values of both convective and impulsive masses (M_0 and M_1 respectively) and their center of mass positions, the method prosed in Housner (1957) as modified in Li and Gou (2018) was adopted. Tanks and fermenters are normally filled to their capacity and then the related FEMs consider them completely full. In addition, considering for the fermenters the presence of a rigid roof preventing the sloshing motion, only the impulsive response of the content was considered. The Figure 3 reports the values of the impulsive and convective mass fraction as function of the ratio H_{wall} / D, obtained for the stock studied in the present work. It is worth to note that convective mass fraction results always smaller than 20% of the total fluid mass in the tank. This is a further confirmation that, the impulsive mass governs the global behaviour of this class of structures.

The study of the dynamic behaviour of the legged vessels, is further complicated by position, stiffness and strength of the legs, all this introducing other variables into the system. The complex vibration modes of these vessels and the fluid-structure interaction produce a wide combination of possible dynamic responses but, on the other hand, few failure mechanisms were detected, for this class of structures, after past earthquakes. As already stated in the introduction, leg buckling, overturning of the whole system and excessive sliding (causing pipes failure and pounding) were the most observed collapse mechanisms. All these mechanisms can have disastrous consequences for both container and content. In Gonzalez et al. (2013) several examples of seismic-induced damage to circular steel legged tanks are reported in detail. Moreover, in several cases local damage was observed at the base of the legs close to the support foots and at the bottom of the vessels (see Figure 1), mainly because of the activation of base-leg uplift and base-leg sliding. These damage mechanisms were detected also very far from the epicentres (more than 100 km from the epicentre) and even if they did not caused tank collapse, they must be evaluated and monitored since they could preclude the regular operation of the tank itself or the on-board equipment (e.g. base support-foot, upper lid, pumps, control panel, pipes and tubes, manholes, level indicator, sampling valve, discharge valve etc.). Based on the information in the aftermath reports cited upon, in the FEM adopted for the seismic analyses, three collapse mechanisms were introduced and monitored:

- tank overturning,
- tank excessive sliding,
- failure of legs or connection legs-mantle,

and two damage mechanisms:

- activation of base-leg uplift,
- activation of base-leg sliding.

The finite element modelling and the activation criteria of the various mechanisms are deeper described in the following Subsection.

2.3 Finite element modelling of the vessels

Numerical analyses were carried out on three-dimensional FEMs of every structure. To this aim, the software OpenSEES was employed (OpenSees 2017). Figure 4a illustrates the main assumptions introduced in the modelling phase. Starting from the expected damage/collapse mechanisms, the numerical models were implemented in order to reliably capture the global dynamic behaviour of the vessels also considering different orientations of the ground-motion entrance direction. At the same time, a computationally efficient model, with few degrees of freedom, was adopted in order to reduce the computational time for the analyses. This aspect will be further detailed in the following Section. The legs and the mantle structures were modelled using elastic finite elements with consistent mass assumption (i.e. the blue elements in Figure 4a). The legs are connected to the mantle element by means of rigid-link elements (i.e. the magenta elements in Figure 4a). A zero-length sliding element (see Single Friction Pendulum Bearing Element in Opensees (2017)) lumped at the base of the legs, introduced the material nonlinearity in the models. The Single Friction Pendulum Bearing Element was selected for simulate the behavior of the leg-pavement contact since – if properly set – it is able to suitably reproduce the leg-pavement contact mechanisms and at the same time proves to be very efficient from a computational point of view. The selected element has coupled friction properties for shear deformation and shear force in the horizontal plane (i.e. the local directions 1 and 2 of the finite element), with horizontal shear force strength (f_{max}) depending from both axial force (i.e. the force along local direction 3) and the type of friction model. In the present work a Coulomb friction model was considered with friction coefficient μ=0.5, independent by the sliding velocity. To capture the uplift mechanism of the bearing element, the material in the axial direction (i.e. dir. 3) has no-tension behavior. The resulting behavior

along the dir. 3 (axial) of the sliding element is detailed in Figure 4c, whereas Figure 4d shows the 3D coupled behavior among the three local directions 1, 2 and 3 of the zero-length elements used here. Then, the axial force on the sliding element results:

$$\begin{cases} f_3 > 0 \quad if \quad d_3 > 0 \\ f_3 = 0 \quad if \quad d_3 \leq 0 \end{cases} \tag{1}$$

and the corresponding horizontal shear force strength (f_{max}) is:

$$f_{max} = \mu \cdot f_3 \tag{2}$$

so, in general, the sliding does not occur if:

$$f_{max} > \sqrt[2]{f_1^2 + f_2^2} \tag{3}$$

In the model, the axial stiffness in compression was set equal to 10^3 kN/mm in order to simulate the stiff support of the usual industrial pavement. Obviously, if during the dynamic analyses, the axial force on a leg becomes equal to zero, also the horizontal shear force strength, for the corresponding leg, becomes zero due to the uplift of the support-foot. On the other hand, higher values of f_3 increase the available force f_{max} preventing the sliding. Until the activation of uplift or sliding mechanism the zero-length element works as extremities hinged to the ground level. The geometrical non-linearity was introduced in the models as well by considering, for the elements, a corotational transformation formulated for large displacements and large rotations (OpenSees 2017).

Masses corresponding to structural dead loads (masses of tank and its components), according to Eurocode 8 (CEN 2005) criteria, were considered as equivalent distributed masses on the beam elements. As far as the fluid mass is concerned, the Housner method (Housner 1957) as modified in Li and Gou (2018) was adopted in order to obtain the convective and impulsive mass values (respectively M_0 and M_1 in Figure 4a), their elevation (respectively H_0 and H_1 in Figure 4a), and the equivalent stiffness K_X and K_Y connecting the convective mass to the mantle walls.

Following the indication in the international codes (CEN 2005; INN Chi 2003) and as largely adopted in the literature on the field (Phan et al. 2017; Colombo and Almazan 2017; Auad and Almazan 2017), a damping ratio ζ_0=2% and ζ_1=0.5% was selected respectively for impulsive and convective masses. The tanks and fermenters were considered completely full, according to their capacity. For the liquid inside the tank, a density equal to 1000 kg/m^3 (or i.e. 1kg/litre) has been assumed. In Table 1 is reported the total mass (Mass) obtained considering both wine and vessel. For the AISI 304L steel class, according to characterization campaign in Gonzalez et al. (2013), a steel yielding stress equal to 310 MPa and an elastic modulus of 193 GPa were assumed. The present FEMs allowed to capture the dynamic global behaviour of the vessels taking into account the fluid-structure interaction. Moreover, this approach allowed the usage of a computationally efficient model able to perform a huge quantity of computationally onerous nonlinear time-history analyses in a reasonable time.

3. SEISMIC INPUT AND DYNAMIC ANALYSES

3.1 Seismic input selection

In order to capture the whole three-dimensional response of a vessel shaken during an earthquake, in the present work the seismic input prescribed at the base of the FEM was represented by three acceleration time-history records acting along the three main directions of the models, i.e. the horizontal directions X, Y and the vertical direction Z (see directions in Figure 4a). A set of ninety recorded acceleration time-histories (60 horizontals and 30 verticals) were selected and extracted from the Pacific Earthquake Engineering Research (PEER) Center strong motion database (PEER 2003) in order to cover a wide range of frequency content, time duration and amplitude, with reference to the horizontal seismic components.

They represent a seismological scenario with moment magnitude (Mw) ranging from 6.5 to 8.0, distance from fault rupture (R) of 6-50 km. The horizontal peak ground acceleration (PGA) ranges from 0.07g to 0.48g; the vertical PGA ranges from 0.04g to 0.37g, recorded on B or C site classes according to Eurocode 8 (CEN 2005). The set considers only records that do not present pulse-velocity shape according to the criteria given in PEER (2013). The main characteristics of the records are reported in Table 2, while Figure 5a shows the horizontal geometric mean (geomean) elastic acceleration response spectra for 5% damping ratio. The red line in the figure indicates the average of the 30 geomean acceleration response spectra (the grey lines). Moreover, none of the records contains near-source effects (i.e. directivity effects). In fact, the two horizontal components (labelled 1 and 2 as in PEER (2003)) of the same event and at the same registration station, have a ratio PGA_1/PGA_2 ranging from 0.5 and 2.0 as showed in Figure 5b and this ratio is not a function of R.

3.2 Time-history dynamic analyses

The dynamic performances of the structures and their sensitivity to seismic excitation were evaluated by IDAs (Vamvatsikos and Cornell 2002). The IDA allows defining median seismic response of the various vessels, for different seismic intensity scenarios, and considering the record-to-record variability of the selected input.

Nowadays, it is not yet clearly defined which seismic intensity measure (IM) has the best performance for sliding-overturning systems since depending from the structure oscillating mechanism (Berto et al. 2018). For example, it is well-known as PGA, for some problems, is much less efficient than others, as for example, the Peak Spectral Acceleration $S_a(T_1)$ for study the collapse of framed buildings (Buratti et al. 2011), or the Peak Ground Velocity (PGV) and Peak Displacement Demand (PDD) in the case of overturning-based failure of free-standing body (Kafle et al. 2011; Petrone et al. 2017). Instead, the definition of the most efficient seismic IM concerning free standing elements with different rigid body motions (i.e. rocking,

overturning, sliding) is still a debated issue (Di Sarno et al. 2017). Moreover, the adoption of spectral acceleration at the first natural period, $S_a(T_1)$, requires the definition of the effective period of the vessel, in case of rocking behaviour, and unfortunately it changes during the dynamic analysis.

In fact, the efficiency of the IM could be case-sensitive depending from the type of collapse mechanism exhibited by the vessel. For this specific work is not possible to define a-priori which is the most efficient IM. Moreover, PGA is still largely used in the literature for the definition of fragility models. In this study the geomean peak ground acceleration ($PGA_{geomean}$) was considered as ground motion IM since it results the most adopted in the tank literature for the definition of fragilities. All this allowing a comparison with the other literature outcomes (Auad and Almazan 2017; Colombo and Almazan 2017). It is worth to note that $PGA_{geomean}$ could be an inefficient IM, especially for some vessel behaviours, therefore it could lead to a high record-to-record variability. Nevertheless, it was adopted here because it is still often adopted in the literature for the definition of fragility models.

The maximum horizontal displacement at the center of mass (C_M) of the tanks (see Figure 4a) was selected as engineering demand parameter (EDP), in order to define the response of the models.

The IDAs were performed by scaling each triad of records starting from a value of IM equal to 0.05g until structural collapse. The structural collapse (associated to ultimate limit state) was identified with the achievement of one of the following mechanisms:

- tank overturning
- tank excessive sliding
- failure of legs.

The collapse mechanisms are illustrated in Figure 6a. As reported in FEMA P-58-1 (FEMA 2012), during earthquakes an unanchored component/structure exhibits an oscillatory

rocking behaviour until the critical displacement is reached, and the objects becomes instable. The critical displacement is the displacement at which the projection of center of mass C_M on the horizontal plane is located over the leading edge. For a system on a discrete supporting system (i.e. the vessels supported by legs), the critical condition is reached when the horizontal projection of C_M is outer the area delimited by the lines connecting two consecutive support-feet.

The collapse for excessive sliding was identified for a horizontal displacement of a support-foot bigger than 20cm. Large displacements in fact, represent the cause of possible connecting pipe failures, pounding among vessels or, even worst, pounding among vessels and facility structures.

The third collapse mechanism was identified as the reaching of yielding stress on the legs. The procedure proposed in EC3 (CEN 2004) for the flexure-axial verification of class-4 sections was taken as reference and implemented in the source script generating the FEM in OpenSEES. In the evaluation of the external bending moment and axial force, obviously also the second order effects were taken into account due to the large values of displacements recorded during the analyses and they were computed in the deformed configuration, following the scheme depicted in Figure 6b, where S indicate the cross-section used to verify the safety of the leg. The attainment of a collapse condition stopped the IDA process. During the IDAs, even two damage mechanisms were monitored, i.e. activation of base-leg uplift and activation of base-leg sliding. These mechanisms could be usefully related to the probability of attainment a serviceability limit state. The first mechanism was identified as soon as the axial force become zero on one leg, the second is activated when at least one of the sliding elements at the base, recorded a displacement higher than 1mm.

In order to obtain the dynamic behaviour of the vessels by considering the possibility of different entrance directions of the ground-motion, different configurations were considered in the numerical analyses. To this purpose, different numerical models, of the same structure,

were produced and analysed. The effect of entrance direction rotation was obtained by rotating the configuration of the legs of the vessels as showed in Figure 4b. So, for the 3-leg vessels 8 configurations were considered. They were obtained by rotating around the vertical axis Z, the legs system of 15° respect to the previous configuration. The same approach was adopted for the 6 configurations of the 4-leg vessels and for the 4 configurations of the 5-legs structures, created by rotating the legs system with increments of 18°. In this way a large set of 25˙800 IDA analyses were performed.

4. INCREMENTAL DYNAMIC ANALYSES RESULTS

4.1 Main characteristics of the IDA curves

The IDA curves here presented, were obtained considering as IM the $PGA_{geomean}$ and, only for convenience, they have on the x-axis the absolute maximum horizontal displacement of C_M. These curves are not sufficient to completely describe the dynamic response of the system under increasing ground-motion, since the different deformation mechanisms (i.e. elastic deformation due to leg-wall flexibility, sliding and rocking) interact during the dynamic oscillatory behavior. As said before, in the present study 25˙800 IDA curves were obtained and adopted for the generation of 420 numerical fragility functions (i.e. 140 vessels for three limit states). The Figure 7a reports, as a representative example, the typical IDA curves provided by time-history analysis for the 4-leg tank #17. Vessels characterized by sliding collapse mechanism (the black line of configuration #1 in the figure) usually have a behavior characterized by a linear phase until the first uplift. After the first uplift, the IDA curves start to become very irregular and oscillating with limited horizontal displacements. The activation of the sliding mechanism typically occurs after few increments of PGA respect to the first uplift and, with the activation of the sliding mechanism, the horizontal displacement of the tank becomes larger and larger until the attainment of the collapse condition. In the picture,

the three limit state conditions of first uplift, first sliding and collapse are identified respectively by the blue, orange and red circles.

4.2 Orientation-induced effects on legged structures

The response of the tanks, in terms of IM, can be significantly influenced by the change of configuration (i.e. by changing the legs orientation). In fact, this aspect can be the responsible for both significant change in the structure capacity (i.e. the collapse PGA) and type of collapse mechanism. For instance, Figure 7a shows that moving from configuration #1 to #3, the 4-leg tank #17 subjected to the same seismic input, exhibits a capacity reduction of 25% in terms of PGA. The sensitive-to-orientation outcomes characterized the dynamic response of several vessels investigated here, all this confirming the need to take into account different ground-motion entrance directions. In general, it was observed that the 3-leg tanks are the most sensitive to the orientation change and the 5-leg structures are the less sensible. In order to prove this, the behavior of a tank for the 30 different triad ground-motions was considered. Figure 7b highlights the different IDA curves provided from the 4-leg tank #19 in configuration #1. In the figure, the red circles identified the collapse (occurring, for this vessel, 6 times for overturning and 4 times for excessive sliding mechanism). Moreover, Figure 7b shows that also the (absolute) value of the collapse displacement C_M is affected by large record-to-record variability for the same tank configuration, ranging around values included between 357mm and 898mm.

Then, in order to set the comparison among the different configurations, all along the IDA process, the median curves for each configuration were computed and compared. So, the grey line depicted in the Figures 7c and d shows the median IDA curves obtained for the different configurations respectively for a 3-leg and a 4-leg tank having similar λ value of 2. As highlight before, due to the change of configuration, the same vessel could collapse with remarkable difference in the horizontal C_M displacement values. To allow a simpler comparison, the current displacements in the figures were normalized by the horizontal displacement at the

collapse PGA value. As discussed before, the 3-legs tank is extremely sensitive to configuration change, and at the collapse the median PGA ranges from $0.45g$ to $0.53g$ (about 18% of difference). The red line in the Figure represents the trend of the total median curve (i.e. the median of the whole IDA curves of the various configurations).

In general, we observed that the higher the number of legs the lower the sensitive-to-orientation collapse capacity of the tank, especially if the overturning mechanism governs the dynamic capacity. This because, on one hand the modification of the legs orientation in the FEMs, does not significantly modify the friction capacity of the tank, but on the other hand, rotating the leg reference system, can change in a considerable way the maximum rotation before the overturning collapse. This outcome becomes clearer considering the specific shape of the non-overturning area (see shaded area in Figure 6a). When the base projection of C_M, for a prescribed rotation, is inside the area, the overturning collapse does not occur. Then, the horizontal displacement capacity is a function of the legs orientation and in general it is not possible to define the most critical direction, but due to the geometry of the problem, as the number of legs increases, the safety area becomes larger and larger, up to the maximum achieved for the infinite-legs theoretical condition. Therefore, in present work, to take into account the possibility that a randomly oriented seismic triad hits the structure, different configurations were considered.

4.3 Collapse mechanism statistics

By analysing the collapse statistics, we observed that the most frequent mechanism was the excessive sliding. This is true for all the three vessel groups (i.e. 3-leg, 4-leg and 5-leg). In fact, as reported in Figure 8a, the excessive sliding collapse occurred in the 83%, 49% and 95% of the whole IDA dataset respectively for 3-, 4- and 5-leg vessels. It is worth to note that, for the most widespread tank typology (i.e. 4-leg), the leg buckling has a significant occurrence percentage, around 40%, and this is comparable to the occurrence of sliding mechanism. On

the contrary, for the 3-leg vessels, the second collapse cause is the tank overturning, with an occurrence percentage around 18%. All this because the 3-leg structures, as already discussed, are the most overturning-sensitive since they have a reduced non-overturning base area. Instead, Figure 8b presents, the most frequent collapse mechanism of each tanks. (i.e. the mechanism with the higher number of occurrences over the 30 time-histories). I.e. for 3-leg, 17 tanks have as most frequent collapse the sliding and 3 the overturning. For the 4-leg, the overturning is the most frequent collapse cause for 5 tanks, whereas 44 returned to be sensitive to leg buckling and 61 to sliding mechanism. If compared to the percentage of 12% in Figure 8a, it emerges that overturning appears in a non-negligible number of IDA analyses but just in few cases represents the major cause of the tank collapse, whereas for the stock considered here, the sliding seems the most frequent mechanism.

In general, we observed that 3-leg vessels showing overturning collapse are those with low mass (lower than 1t) but at the same time characterized by valuable slenderness (λ around 2). For these, the overturning anticipated the other mechanisms, whereas for the vessels with mass higher than 1t, the sliding mechanism was the most demanding. For the 4-leg vessels instead, we observed the overturning collapse mechanism mainly in structure with mass ranging from 0t to 5t, sliding in those having masses between 5t and 30t and limited λ values, lower than 3. Then, leg buckling was the main collapse cause for the high capacity vessels with mass higher than 30t. Similar conclusion can be drawn also for 5-leg cases but in this group, the absence of vessels with mass higher than 30t and lower than 5t, excluded the leg buckling and the overturning and only sliding collapse mechanism were observed.

This consideration could result rather useful to plan the most effective retrofitting interventions to improve the safety of the vessels. Finally, Figure 8c shows the median collapse PGA values computed for each tank by considering the whole outcome set coming from the time-histories performed for the various configurations. How Figure 8c, highlights the median PGA ranges are $0.20g$ - $0.45g$, $0.09g$ - $0.51g$ and $0.47g$ - $0.55g$ respectively for the 3,

4 and 5-leg structures. Then, it is not possible to find a reliable relation between PGA values and collapse mechanism. Since the PGA bands are comparable for the various collapse mechanisms and by comparing the results from the various IDA curves, a PGA-mechanism correlation cannot be found. Finally, in general, it is not possible to identify the tank group with the highest seismic sensitivity.

5. FRAGILITY FUNCTIONS

5.1 Fragility function hypotheses

The IDA data processing started with the definition of the fragility functions associated to each tank. Following a consolidated method, the cumulative fraction of structures attaining a prescribed damage state, expressing the probability of exceeding that damage state, were estimated for increasing levels of the IM, providing the fragility distribution. The fragility function for a specific damage state F(·) is assumed to be a lognormal cumulative distribution function:

$$F(s) = \Phi\left[\frac{ln\left(\frac{s}{\mu}\right)}{\sigma}\right] \tag{4}$$

where: s represents $PGA_{geomean}$ and Φ[·] is the standardized normal cumulative distribution function. The values of the two parameters μ and σ in Eq.(4), describing the fragility function, can be estimated using different methods (Buratti et al. 2017). In the present paper the maximum likelihood estimation method was used. By adopting the same nomenclature used in Bovo and Buratti (2019), the maximum likelihood function $L(\mu,\sigma \mid \mathbf{Y})$ can be defined as:

$$L\left(\mu,\sigma \mid \mathbf{Y}\right) = \prod_{i=1}^{N} \frac{1}{\sqrt{2\pi\sigma^2}} \exp\left(\frac{-\left(\ln\left(y_i\right)-\mu\right)^2}{2\sigma^2}\right) \tag{5}$$

where: the vector **Y** contains N values y_i corresponding to the N values of IM (i.e. $PGA_{geomean}$) obtained from the IDA, for the considered limit state (i.e. uplift, sliding or collapse). The estimates of the fragility model parameters (μ and σ) are those maximizing the likelihood function. The value of μ and σ have been computed by adopting an optimization algorithm for the maximization of $ln\ L$ and hence L by imposing:

$$\frac{\partial\, ln\, L}{\partial\, \mu} = \frac{\partial\, ln\, L}{\partial\, \sigma} = 0 \tag{6}$$

Further details on the likelihood function method can be found in Lallemant (2015), Bovo and Buratti (2019), Tothong and Luco (2007), Koutsourelakis et al. (2003), Shinozuka (2000) and are not reported here for the sake of brevity.

In order to generate fragility functions as general as possible and not affected by ground motions biases (i.e. fragility functions non-depending on the input ground motions or, as in this case, non-depending on the ground-motion entrance direction), the dataset used for the generation of fragility functions was constituted by all the available IM values obtained for a specific condition (i.e. limit state) from the various configurations. So, for the generation of 3-leg tank fragility functions, a data set of 240 PGA values was considered (i.e. 8 configurations × 30 different seismic input), while the set collects 180 and 120 PGA values respectively for 4-leg and 5-leg tanks (i.e. respectively 6 and 4 configurations × 30 seismic input).

This approach follows the hypothesis that dynamic responses evaluated for the various directions have the same probability of occurrence (i.e. they are isoprobable). By following this approach, we have both pros and cons. The first (negative) consequence, occurs when these fragilities are applied in loss assessment analyses, since this approach can slightly underestimate (or overestimate) the probability of exceedance (POE) and consequently the seismic losses, if the tanks of a stock have same legs orientation. In fact, the fragilities assume a random oriented stock. Second, we introduced in the fragility functions also the orientation-variability and, consequently, the lognormal fitting functions could be characterized by more dispersion than those obtained for a single configuration in which the record-to-record variability only is usually present. Moreover, for the studied structures, the introduction of the directionality in the fragility functions can appear useless, since the directionality in the dynamic responses is not correlated to a directional IM. In fact, the IM assumed in the present work, $PGA_{geomean}$, has no directionality. Moreover, we have the further complication that the configuration showing the worst dynamic performance (i.e. the configuration providing the

lowest PGA values) changes during the IDA analyses, with the seismic intensity level, so at the present it is impossible to define a-priori the worst configuration of a tank.

However, the approach so far described could be extended by considering different weights for the various configurations. These weights could be defined based on expert opinion and engineering judgment in order to provide more conservative (i.e. on the safety side) fragilities if particular seismic scenarios are to be considered. In order to include them in the fitting procedure, the easiest approach is resampling structural capacity data proportionally to the importance weights, thus increasing the number of terms in the likelihood function. It should be noticed that the judgement of different experts could be easily combined using logic tree. This further extension is not introduced in the present work since is out of the scope of the work.

5.2 Main outcomes

Table 3, reported in the Appendix, collects the median values (e^{μ}), the standard deviation values (σ) and the coefficient of determination R^2 of the fitting lognormal distribution of the fragility models, for the three considered limit state conditions (collapse, activation of base-leg uplift and activation of base-leg sliding).

As example, Figure 9 shows the fragility curves of a 3-, 4- and 5-leg tanks (respectively #15, #4 and #3) whose have similar geometrical parameters and are all characterized by λ about 2. The three tanks have comparable fragilities, for every limit state, with a slight increase in the median PGA value at the collapse by moving from 3- to 5-leg (i.e. from 0.41g to 0.46g). Differently, referring to the damage conditions, the median PGA values are very similar, and they range around 0.11g-0.13g for the uplift condition and 0.13g-0.16g for the sliding activation. As frequently observed in the present stock, the sliding mechanism activates few PGA increments after the uplift, whereas the opposite situation (uplift after the sliding) occurs rarely.

In general, the structure capacity e^{μ} at the collapse has values ranging from 1 to 4 times those observed for the damage conditions. The collapse, on average, occurs for acceleration 2.5 times higher than those causing the damage conditions. From the evaluation of the results in terms of fragility dispersion, it emerges that the value of σ increases by moving from the uplift to the sliding, and then to the collapse state. But the growth is rather limited since, e.g. for 4-leg tanks it moves from a value of 0.18 at uplift to 0.22 of sliding, and then 0.25 at the collapse. This result confirms the general expectation that an increase of IM leads to a large scatter of the output around the median due to nonlinearity of the structures. The good fitting between numerical and analytical fragility functions is testified by the high values of the coefficient of determination (i.e. R^2 according to Montgomery et al. (2010)), always higher than 0.85 (see Table 3).

It seems worth to note that from a preliminary comparison with the fragility functions provided in other study, for anchored legged tanks (Colombo and Almazan 2017; Auad and Almazan 2017), at collapse and for POE=0.5 (i.e. e^{μ}), PGA values are quite close to those obtained in the present work. From these emerging outcomes seems that the introduction of a fixed anchoring system at the base, do not change the final seismic capacity of the existent legged tanks. This because, even though in anchored tanks sliding and overturning collapse mechanisms are not allowed because of the base restraints, in anchored vessels other damage mechanisms can be observed. For instance the buckling of tank walls and legs, the failure of the anchorage system caused by high base-overturning moment and damage to the shell-base connection caused by the plastic rotation of the base plate of the tank (Colombo and Almazan 2017). So, it seems that in existent tanks, the presence of a base anchoring system anticipated the appearance of some collapse modes (i.e. buckling of the legs and rupture of the shell-base connection) and resulting similar seismic capacities between anchored and unanchored tanks. This aspect will be object of future investigations aimed at comparing the different dynamic features distinguishing the anchored from the unanchored existing tanks.

Finally, the next Section will introduce and explain the analytical expressions for the definition of the fragility curves of unanchored cylindrical steel legged tanks starting from the knowledge of few geometrical information. These expressions will provide a practical and meaningful tool for the evaluation of the seismic sensitivity of a vessel. These, obviously, will also allow fast recognition of the seismic vulnerability of the main equipment in a winemaking/storage agricultural facility.

6. RESPONSE SURFACE PROPOSAL FOR FRAGILITIES DEFINITION

6.1 Response surface features

The availability of the fragilities of a large sample of tanks, characterized by wide range of geometries and capacities, represents an interesting and statistically representative data set. In fact, the parameters (i.e. e^{μ} and σ) of the best fitting lognormal function of every tank, for each limit state, were statistically elaborated to define a reliable response surface (RS) for the distribution parameters. According to the description provided in Buratti et al. (2010) the response surface method is based on the definition of a statistical model expressing the values of a response parameter as a function of a set of variables. Usually, the RS is defined as a polynomial function and the method was adopted in the past in several research fields (Khuri and Cornell 1996; Searle 1992). In this work, the response parameters, approximated by means of response surface, were e^{μ} and σ referred to a specific limit state condition. So, in the present paper, six RSs were defined (2 parameters × 3 limit states).

In the RS method, the expected value E(Y) of a response parameter Y is approximated by a polynomial function, usually up to the second degree (Khuri and Cornell 1996), of a set of factors x:

$$E(Y)=f(x)^{T}\,\alpha \tag{7}$$

where f(x) is a n×1 vector of the monomials of x (e.g. $f(x)^T = [\ 1, x_1, \ldots, x_j, x_1 \cdot x_1, x_1 \cdot x_2, \ldots, x_j \cdot x_j\ ]$) and α is the vector collecting the n regression parameters. The residual (or error in the prediction) of the ith observation Y_i from the expected value $E(Y_i)$ can be expressed as:

$$r_i = Y_i - E(Y_i) = Y_i - f(x_i)^T \alpha \quad (\text{with } i=1, \ldots, N) \tag{8}$$

Therefore, considering the whole set of N observations, the model in Eq. (8) can be expressed, in matrix notation, as:

$$Y = \mathbf{X}\,\alpha + r \tag{9}$$

where $Y^T = [Y_1, \ldots, Y_N]$, $\mathbf{X}$ is an N × n matrix whose i th row is the vector of monomials $f(x)^T$ calculated for the values assumed by the factors x at the ith point and $r = [r_1, r_2, \ldots, r_N]^T$ is the vector collecting the residuals of Y_i with respect to $E(Y_i)$. The regression parameters α in Eq. (9) can be estimated using least squares or maximum likelihood methods.

6.2 Response surface definition and calibration

During the process for the most influential factor identification (candidate assessment) for the structures at hand, several factors and related combinations were considered and tested to search the combination that provides the maximum R^2_{adj} (Montgomery et al. 2010) under the conditions pValue < 0.1 for all the factors (Montgomery et al. 2010) and with absolute value extra-diagonal terms in the variance-covariance matrix lower than the corresponding diagonal terms, i.e. $\sigma_{ij} < \sigma_{ii}$ and $\sigma_{ij} < \sigma_{jj}$ for every i,j (Searle et al. 1992). In this way, we searched for a sufficient, complete and weakly dependent factors set. During the candidate assessment procedure we considered the following 12 candidates: M, D, λ, β, γ, Γ, M^2, D^2, λ^2, β^2, γ^2 and Γ^2 (with: M: mass of tank and fluid; D: tank diameter; $\lambda = H/D$; $\beta = H_{wall}/H_{leg}$; $\gamma = H_{wall}/D$; $\Gamma = M/H_{wall}$) in order to introduce possible linear and quadratic dependence. We started by adding one candidate at time following the list above. If the new candidate increases the R^2_{adj} and at the same time respects the conditions on pValue and on the extra-diagonal terms in the variance-covariance matrix, the candidate is added in the adjusted

version of the fitting equation. If the candidate does not respect the prescribed conditions, is removed from the equation and the procedure moves forward by assessing the following candidate.

Four candidates (i.e. factors) resulted sufficient to obtain a good fitting between analytical and numerical data for both e^{μ} and σ. The selected factors were: λ (H/D ratio), M (mass of tank and fluid), D (diameter), Γ (M/H_{wall} ratio). The best fitting equations for e^{μ} and σ resulted:

$$e^{\mu}\,[g] = a_0 + a_1\,\lambda + a_2\,\lambda^2 + a_3\,M + a_4\,M^2 \tag{10}$$

$$\sigma\,[g] = b_0 + b_1\,D + b_2\,\lambda + b_3\,M + b_4\Gamma \tag{11}$$

As an example, Figure 10 shows e^{μ} distribution, for the different limit states of 4-leg group, as a function of λ and mass M. The uplift and sliding conditions have an almost parabolic trend respectively with λ (Figure 10a-b) and with M (Figure 10d-e) even if the variation of e^{μ} is rather limited for these damage conditions (about from 0.1g to 0.2g). The collapse limit state has more irregular trend (see Figure 10c and f) due to the interaction of the different collapsing causes, occurring for different mechanisms. It is worth noting as for the lower mass values (0t-5t), e^{μ} ranges from 0.2g to 0.4g and corresponds to an overturning collapse mechanisms in several cases. For higher mass values until about 30t, the main collapse mechanism is the sliding and for mass values higher than 30t the primary collapse cause is the leg buckling. In this way we can try to depict a transition on the collapse mechanism for increasing mass values.

The apparent low correlation resulting in Figure 10c and f justifies the adoption of a multi-factors response surface. Similar conclusion on the dispersion of the points can be drawn by analysing the distribution of $\sigma_{collapse}$ vs. the factors D, λ, M and Γ reported in Figure 11 for the 4-leg tanks. Moreover, a further cause of dispersion can be attributed to the choice of the IM as reported in Section 3.

By means of least squares regression procedure, the value of the 10 regression parameters (i.e. a_0-a_4 and b_0-b_4) in Eq. (10) and Eq. (11) were evaluated for the different limit states. They are reported respectively in Table 4 and 5 together with the values of R^2_{adj}. The coefficient of determination is rather high for the median, ranging from 0.75 to 0.99. The values of R^2_{adj} for sigma are slightly lower resulting between 0.70 and 0.91. Following the Eq.(10) it is possible to graphically represent, in a three-dimension space, the RS for the median, since only two factors are present and the RS has the general form z=f(x, x^2, y, y^2) (i.e. e^{μ}=f(λ, λ^2, M, M^2)). The RS of the 4-leg tank collapse and uplift median e^{μ} are plotted in Figure 12a and b respectively. The shapes are rather similar for the other tank groups as well and, as the figure shows, a second order equation prove to be adequate enough to fit the numerical data. The graphs related to other vessel groups and limit state conditions are not reported here for the sake of brevity. On the other hand, plotting in a univocal way the RS surfaces of the dispersion σ is not possible, since σ=f(D, λ, M, Γ) results a function in a five-dimension space.

The Eq.s(10)-(11) together with the parameter values in Tables 4 and 5 provide a practical and meaningful tool for the evaluation of the fragilities of particular legged vessel typologies. These, obviously, will also allow fast recognition of the seismic vulnerability of the main equipment in a winemaking/storage agricultural facility since, in order to apply the expressions, only 4 geometrical tank data are needed (i.e. D, M, H, H_{wall}).

7. FINAL REMARKS

The circular steel legged tanks are maybe the vessel class most used worldwide in the wine making and storage processes. At the same time, they represent a structural typology very sensitive to seismic excitation, as some major earthquakes revealed. The direct and indirect high seismic-induced losses that some recent major earthquakes produced on the wine industry, motivated the present study and the definition of fragility curves for a high number

of existing legged tanks. So, starting from the collection of a large stock of some of the most widespread unanchored vessels, the fragility curves of three groups of steel legged, i.e. 3-, 4- and 5-leg, tanks were obtained by means of IDAs on nonlinear FEMs. Three different limit states were monitored during the dynamic analyses. The first is connected to the activation of the uplift mechanism, the second concerns the activation of the first sliding phenomenon, the third governs the structure collapse and was identified as the tank overturning, or in alternative, as the base-tank excessive sliding or again the leg collapse. 140 unanchored vessels were modelled and analysed in different configurations under the prescription of a seismic ground motion triad, scaled until collapse in terms of geomean PGA of the two horizontal components. 25˙800 IDA curves were created and adopted for the generation of 420 empirical fragility functions (i.e. 140 vessels for three limit states).

As far as the tank dynamic behavior is concerned, during ground-motion, after the first leg uplift, the dynamic behavior initiate to become very instable and the tank oscillates with limited horizontal displacements. The activation of the sliding mechanism typically occurs after few increments of PGA respect to the first uplift and, with the activation of the sliding mechanism, the horizontal displacement of the tank becomes larger and larger as far as the reaching of the collapse condition. Therefore, the response of the tanks, in terms of capacity, can significantly change according to the seismic entrance direction. In general, we observed that the higher the number of legs the lower the sensitivity-to-orientation collapse capacity of the tank, especially when the overturning mechanism governs the dynamic capacity. By analysing the collapse statistics, it is noticeable that the most frequent mechanism is the excessive sliding occurring for 3-, 4- and 5-leg structures respectively in the 83%, 49% and 95% of the whole IDA data set.

Moreover, for the 4-leg structures, the leg buckling has a significant occurrence percentage, around 40%, being comparable to occurrence of sliding mechanism. The seismic analyses confirm the sensitivity of this class of tanks providing median PGA ranges of 0.20g - 0.45g,

$0.09g$ - $0.51g$ and $0.47g$ - $0.55g$ respectively for the 3-, 4- and 5-leg structures. Then, by comparing the collapse PGAs emerging by the present work with those from literature for anchored vessels, we observed that the values are quite similar, even if the collapse mechanisms are very different. This aspect will be object of future investigation aimed to compare the different dynamic features distinguishing the anchored from the unanchored existing tanks.

By processing the IDA outcomes, the empirical fragilities were achieved and then fitted by means of lognormal cumulative distribution functions whose statistical parameters (median e^{μ} and dispersion σ) were properly assessed by maximum likelihood method. The values of the parameters of the lognormal function of every tank, for each limit state, were statistically elaborated in order to define a reliable response surface for the distribution parameters. The four selected factors, i.e. λ (H/D ratio), M (mass of tank and fluid), D (diameter) and Γ (M/H_{wall} ratio), resulted to be a sufficient, complete and weakly dependent set and then they were introduced in the analytical expressions of the response surfaces of statistical parameters e^{μ} and σ.

The analytical expressions provided in the present paper, proved to be a practical and useful tool for the evaluation of the fragilities of legged vessels having characteristics similar to those investigated here. The analytical response surfaces, obviously, will also allow fast recognition of the seismic vulnerability of the tank equipment in a win-making/storage agricultural facilities since few geometrical data are needed to apply the expressions.

REFERENCES

ASTM (2018) A240/A240M-18 Standard Specification for Chromium and Chromium-Nickel Stainless Steel Plate, Sheet, and Strip for Pressure Vessels and for General Applications ASTM International, West Conshohocken, PA.

Auad GA, Almazan JL (2017) Non linear vertical-rocking isolation system: Application to legged wine storage tanks. Engineering Structures 152:790-803.

Berahman F, Behnamfar F (2007) Seismic Fragility Curves for Un-Anchored On-Grade Steel Storage Tanks: Bayesian Approach. Journal of Earthquake Engineering 11(2):166-192.

Berto L, Rocca I, Saetta A (2018) Vulnerability assessment methods for rocking and overturning of free standing elements. Soil Dyn Earthq Eng 110. doi:10.1016/j.soildyn.2018.02.010.

Bovo M, Buratti N (2019) Evaluation of the variability contribution due to epistemic uncertainty on constitutive models in the definition of fragility curves of RC frames. Engineering Structures 188:700-716.

Brunesi E, Nascimbene R, Pagani M, Beilic D (2014) Seismic Performance of Storage Steel Tanks during the May 2012 Emilia, Italy, Earthquakes. Journal of Performance of Constructed Facilities 29(5). doi:10.1061/(ASCE)CF.1943-5509.0000628.

Buratti N., Ferracuti B., Savoia M. (2010) Response Surface with random factors for seismic fragility of reinforced concrete frames. Structural safety 32:42-51. ISSN: 0167-4730.

Buratti N, Stafford PJ, Bommer JJ (2011) Earthquake accelerogram selection and scaling procedures for estimating the distribution of drift response. Journal of Structural Engineering, 137(3), 345–357. https://doi.org/10.1061/(asce)st.1943-541x.0000217.

Buratti N, Tavano M (2014) Dynamic buckling and seismic fragility of anchored steel tanks by the added mass method. Earthquake Engng Struct. Dyn. 43:1–21.

Buratti N, Minghini F, Ongaretto E, Savoia M, Tullini N (2017) Empirical seismic fragility for the precast RC industrial buildings damaged by the 2012 Emilia (Italy) earthquakes. Earthquake Engng Struct. Dyn 46:2317-2335. doi: 10.1002/eqe.2906.

CEN (European Committee for Standardization) (2004) Eurocode 3-Part 1: General rules and rules for buildings. Brussels, Belgium.

CEN (European Committee for Standardization) (2005) Eurocode 8: General rules, seismic actions and rules for building. Brussels, Belgium.

Colombo JI, Almazan JL (2017) Seismic reliability of legged wine storage tanks retrofitted by means of a seismic isolation device. Engineering Structures 134:303-316.

Cooper D (2004) A history of steel tank structural design. Wine Business Monthly, July.

Di Sarno L, Magliulo G, D'Angela D, Cosenza E (2019) Experimental assessment of the seismic performance of hospital cabinets using shake table testing. Earthq Eng Struct Dyn 2019;48:103-23. doi:10.1002/eqe.3127.

Dizhur D, Simkin G, Giaretton M, Loporcaro G, Palermo A, Ingham J (2017) Performance of winery facilities during the 14 November 2016 Kaikoura earthquake. Bulletin of the New Zealand Society for Earthquake Engineering 50(2).

EERI Reconnaissance Team (1990) Loma Prieta Earthquake Reconnaissance Report. Earthquake Spectra 6: 189–238.

EERI Reconnaissance Team (2004) Preliminary observations on the December 22, 2003, San Simeon Earthquake. EERI Special Earthquake Report, March.

FEMA (Federal Emergency Management Agency) (2012) Seismic Performance Assessment of Buildings: Volume 1 – Methodology, FEMA P-58-1.

Gonzalez E, Almazan J, Beltran J, Herrera R, Sandoval V (2013) Performance of stainless steel winery tanks during the 02/27/2010 Maule Earthquake. Eng Struct 56:1402-18.

Hamdan FH (2000) Seismic behaviour of cylindrical steel liquid storage tanks. Journal of Constructional Steel Research 53(3):307–333.

Haroun MA, Housner GW (1981) Earthquake response of deformable liquid storage tanks. Journal of Applied Mechanics 48(2):411–417.

Haroun MA, Housner GW (1982) Complications in Free Vibration Analysis of Tanks. Journal of Engineering Mechanics Division, ASCE, Vol. 108(EM5):801-818.

Haroun MA, Ellaithy HM (1985) Model for Flexible Tanks Undergoing Rocking. Journal of Engineering Mechanics, ASCE 111(2):143-157.

Haroun MA, Tayel MA (1985) Axisymmetrical Vibrations of Tanks-Analytical. Journal of Engineering Mechanics, ASCE 111(3):346-358.

Housner GW (1957) Dynamic pressure on accelerated fluid containers. Bulletin of the Seismological Society of America 47(1):15–35.

Housner GW (1963) The dynamic behaviour of water tanks. Bulletin of the Seismological Society of America 53 (1):381–387.

Hunt B, Priestley MJN (1978) Seismic water waves in a storage tank. Bulletin of the Seismological Society of America 68(2):487–499.

Iervolino I, Fabbrocino G, Manfredi G (2004) Fragility of standard industrial structures by a response surface based method. Journal of Earthquake Engineering, 8(6):927–945.

INN Chi (Instituto Nacional de Normalizacion Chile) (2003) NCh 2369 Of 2003 Earthquake resistant design of industrial structures and facilities. Santiago (Chile): Instituto Nacional de Normalización.

Italian Wine Central (2019) Top Fifteen Wine-Producing Countries; https://italianwinecentral.com/top-fifteen-wine-producing-countries, website (last access January 2019).

Jacobsen LS (1949) Impulsive hydrodynamics of fluid inside a cylindrical tank and of fluid surrounding a cylindrical pier. Bulletin of the Seismological Society of America 39(3):189–204.

Kafle B, Lam NTK, Gad EF, Wilson J (2011) Displacement controlled rocking behaviour of rigid objects. Earthq Eng Struct Dyn 40:1653-69. doi:10.1002/eqe.1107.

Khuri AI, Cornell JA (1996) Response surfaces: designs and analyses. New York: Marcel Dekker.

Koutsourelakis PS, Pradlwarter HJ, Schuëller GI (2003) Reliability of structures in high dimensions. Proceedings in Applied Mathematics and Mechanics 3(1):495–496.

Lallemant D, Kiremidjian A, Burton H (2015) Statistical procedures for developing earthquake damage fragility curves. Earthquake Engineering and Structural Dynamics. https://doi.org/10.1002/eqe.2522.45.

Leon GS (1986) Seismic Analysis of Fluid Storage Tanks. Journal of Structural Engineering, ASCE 112(1):1-18.

Li YC, Gou HL (2018) Modeling problem of equivalent mechanical models of a sloshing fluid. Shock and Vibration. Article ID 2350716. https://doi.org/10.1155/2018/2350716.

Manos G (1991) Evaluation of the earthquake performance of anchored wine tanks during the San Juan, Argentina, 1977 Earthquake. Earthquake Eng Struct Dyn 20:1099–114.

Montgomery D, Runger G, Hubele N (2010) Engineering Statistics (5° Ed.) John Wiley & Sons. ISBN 0470631473.

Niwa A, Clough R (1982) Buckling of cylindrical liquid-storage tanks under earthquake loading. Earthquake Eng Struct Dyn 10:107–22.

OpenSees (Open System for Earthquake Engineering Simulation) (2017) Command manual, Website http://opensees.berkeley.edu/wiki/index.php/Command_Manual.

PEER (Pacific Earthquake Engineering Research Center) (2003) Structural Performance Database Website, http://nisee.berkeley.edu/spd/index.html.

PEER (2013) Final Report of the NGA-West2 Directivity Working Group, PEER Report 2013/09.

Petramale LL (2019) www.petramaleacciai.com, website (last access January 2019).

Petrone C, Di Sarno L, Magliulo G, Cosenza E (2017) Numerical modelling and fragility assessment of typical freestanding building contents. Bull Earthq Eng 15:1609-33. doi:10.1007/s10518-016-0034

Phan HN, Paolacci F, Alessandri, S (2016) Fragility analysis methods for steel storage tanks in seismic prone areas. In: Proceedings of ASME 2016 Pressure Vessels and Piping Conference, Vancouver, British Columbia, Canada, Vol. 8. http://dx.doi.org/10.1115/PVP2016-63102.

Phan HN, Paolacci F, Bursi OS, Tondini N (2017) Seismic fragility analysis of elevated steel storage tanks supported by reinforced concrete columns. Journal of Loss Prevention in the Process Industries 47:57-65.

Rammerstorfer FG, Scharf K, Fisher FD (1990) Storage Tanks Under Earthquake Loading. Applied Mechanics Reviews 43(11):261–282.

Salzano E, Iervolino I, Fabbrocino G (2003) Seismic risk of atmospheric storage tanks in the framework of quantitative risk analysis. Journal of Loss Prevention in the Process Industries 16:403-409.

Searle SR, Casella G, McCulloch CE (1992) Variance components. New York: John Wiley and Sons.

Shinozuka M, Feng MQ, Lee J, Naganuma T (2000) Statistical analysis of fragility curves. Journal of EngineeringMechanics 126(12):1224–1231.

Swan W, Miller D, Yanev P (1984) The Morgan hill earthquake of April 24, 1984 - effects on industrial facilities, buildings, and other facilities. Earthquake Spectra 1:457–568.

Taucer F, Alarcon J, So E (2008) 2007 August 15 Magnitude 7.9 earthquake near the Central Coast of Central Peru. Edited by Fabio Taucer. Joint Research Centre Scientific and Technical Reports. EUR 23359 EN. Luxembourg: Office for Official Publications of the European Communities.

Tothong P, Luco N (2007) Probabilistic seismic demand analysis using advanced ground motion intensity measures. Earthquake Engineering and Structural Dynamics 36(13):1837-1860.

Vamvatsikos D, Cornell CA (2002) Incremental dynamic analysis. Earthquake Engng Struct. Dyn. 31:491–514. doi: 10.1002/eqe.141.

Veletsos AS, Yang JY (1977) Earthquake response of liquid storage tanks. In Advances in Civil Engineering through Engineering Mechanics - Second Annual Engineering Mechanics Division Specialty Conference, ASCE: North Carolina State University, Raleigh, North Carolina, U.S.A. pp.1–24.

Veletsos AS (1984) Seismic response and design of liquid storage tanks in Guidelines for the Seismic Design of Oil and Gas Pipeline Systems. Committee on Gas and Liquid Fuel Lifelines of the ASCE Technical Council on Lifeline Earthquake Engineering Ed., ASCE: New York.

Veletsos AS, Shivakumar P (1997) Dynamic response of tanks containing liquids or solids. In Computer Analysis and Design of Earthquake Resistant Structures DE Beskos and SA Anagnostopoulos, Ed. Computational Mechanics, Inc.

APPENDIX

The Appendix collects the main geometrical characteristics of the vessels considered in the present study (Table 1). Moreover, the fitting lognormal distribution parameters for the various limit states analysed in the work are reported in Table 3.

Table 1. Main geometrical characteristics of the vessel stock.

3-leg vessels

#	Vessel type*	H_{wall} [mm]	D [mm]	C [m^3]	H_{leg} [mm]	Leg type**	Leg cross-section	Mass [t]	λ [-]
1	T	1000	636	0.3	400	S	250×250 - t=2	0.33	2.20
2	T	1000	724	0.4	400	S	250×250 - t=2	0.44	1.93
3	T	1250	724	0.5	400	S	250×250 - t=2	0.54	2.28
4	T	1250	794	0.6	400	S	250×250 - t=2	0.65	2.08
5	T	1250	858	0.7	400	S	250×250 - t=2	0.75	1.92
6	T	1250	928	0.8	400	S	250×250 - t=2	0.86	1.78
7	T	1250	1020	1.0	400	S	250×250 - t=2	1.06	1.62
8	T	2000	1194	2.0	500	CT	∅ 300 - t=2.5	2.12	2.09
9	T	2000	1430	3.0	500	CT	∅ 300 - t=2.5	3.14	1.75
10	T	2500	1593	5.0	500	C	∅ 300 - t=2.5	5.20	1.88
11	T	3000	2070	10.0	500	C	∅ 300 - t=2.5	10.31	1.69
12	T	4500	2388	20.0	500	S	300×300 - t=2.5	20.53	2.09
13	T	6250	2500	30.0	500	S	300×300 - t=2.5	30.77	2.70
14	FE	2000	1430	3.4	500	S	300×300 - t=2.5	3.54	1.75
15	FE	2500	1430	4.2	500	S	300×300 - t=2.5	4.38	2.10
16	FE	3000	1430	5.0	500	S	300×300 - t=2.5	5.21	2.45
17	FE	2000	1600	4.3	500	S	300×300 - t=2.5	4.46	1.56
18	FE	2500	1600	5.3	500	S	300×300 - t=2.5	5.50	1.88
19	FE	3000	1600	6.3	500	S	300×300 - t=2.5	6.54	2.19
20	FE	5500	2400	25.0	500	S	300×300 - t=2.5	25.65	2.50

4-leg vessels

#	Vessel type*	H_{wall} [mm]	D [mm]	C [m^3]	H_{leg} [mm]	Leg type**	Leg cross-section	Mass [t]	λ [-]
1	T	1500	1150	1.5	400	ST	250×250 - t=2.5	1.59	1.65
2	T	1500	1320	2.0	400	ST	250×250 - t=2.5	2.10	1.44
3	T	2000	1274	2.5	400	ST	250×250 - t=2.5	2.63	1.88
4	T	2500	1400	3.8	400	ST	250×250 - t=2.5	3.97	2.07
5	T	2000	1592	4.0	400	ST	250×250 - t=2.5	4.16	1.51
6	T	2500	1592	5.0	400	ST	250×250 - t=2.5	5.20	1.82
7	T	2500	1740	6.0	400	ST	250×250 - t=2.5	6.21	1.67
8	T	3000	1740	7.0	400	ST	250×250 - t=2.5	7.26	1.95
9	T	3000	1840	8.0	400	ST	250×250 - t=2.5	8.27	1.85
10	T	3000	2100	10.0	400	ST	250×250 - t=2.5	10.31	1.62
11	T	3000	2500	15.0	400	ST	250×250 - t=2.5	15.37	1.36
12	FE	4480	2388	20.0	500	C	∅ 300 - t=2.5	20.53	2.09
13	FE	6650	2400	30.0	500	C	∅ 300 - t=2.5	30.79	2.98
14	T	4480	2388	20.0	500	CT	∅ 300 - t=2.5	20.53	2.09
15	T	5900	2547	30.0	500	CT	∅ 300 - t=2.5	30.74	2.51
16	T	6250	2866	40.0	500	CT	∅ 300 - t=2.5	40.88	2.36
17	T	8500	3000	60.0	500	CT	∅ 300 - t=2.5	61.26	3.00
18	FE	1250	1020	1.0	300	ST	300×300 - t=2.5	1.06	1.52
19	FE	1870	1020	1.5	300	ST	300×300 - t=2.5	1.59	2.13

20	FE	2500	1020	2.0	300	ST	300×300 - t=2.5	2.13	2.75
21	FE	2000	1200	2.0	600	ST	300×300 - t=2.5	2.12	2.17
22	FE	2000	1400	3.0	600	ST	300×300 - t=2.5	3.14	1.86
23	FE	2500	1600	5.0	600	ST	300×300 - t=2.5	5.20	1.94
24	FE	3750	1600	7.7	600	ST	300×300 - t=2.5	8.00	2.72
25	FE	2500	2000	8.0	600	ST	300×300 - t=2.5	8.25	1.55
26	FE	3500	2000	10.0	600	ST	300×300 - t=2.5	10.35	2.05
27	FE	3500	2390	15.0	600	ST	300×300 - t=2.5	15.41	1.72
28	FE	4250	2500	20.0	600	ST	300×300 - t=2.5	20.52	1.94
29	FE	6250	2500	30.0	600	ST	300×300 - t=2.5	30.77	2.74
30	T	2500	1020	2.0	600	CT	∅ 300 - t=2.5	2.13	3.04
31	FE	1500	1600	3.1	500	ST	300×300 - t=2.5	3.22	1.25
32	FE	3000	1450	5.0	500	ST	300×300 - t=2.5	5.21	2.41
33	FE	2000	1950	6.1	500	ST	300×300 - t=2.5	6.29	1.28
34	FE	4000	1950	12.0	500	ST	300×300 - t=2.5	12.38	2.31
35	FE	2000	2300	8.5	500	ST	300×300 - t=2.5	8.73	1.09
36	FE	2500	2300	10.5	500	ST	300×300 - t=2.5	10.78	1.30
37	FE	3000	2300	12.6	500	ST	300×300 - t=2.5	12.94	1.52
38	FE	4000	2300	16.8	500	ST	300×300 - t=2.5	17.25	1.96
39	FE	4500	2300	18.9	500	ST	300×300 - t=2.5	19.41	2.17
40	FE	5000	2300	20.9	500	ST	300×300 - t=2.5	21.47	2.39
41	FE	4500	2540	23.1	600	ST	300×300 - t=2.5	23.66	2.01
42	FE	5000	2960	25.7	600	ST	300×300 - t=2.5	26.43	1.89
43	FE	3000	2960	21.1	600	ST	300×300 - t=2.5	21.54	1.22
44	FE	3500	2960	24.6	600	ST	300×300 - t=2.5	25.11	1.39
45	FE	4000	2960	28.0	600	ST	300×300 - t=2.5	28.58	1.55
46	FE	4500	2960	31.5	600	ST	300×300 - t=2.5	32.16	1.72
47	FE	5000	2960	34.9	600	ST	300×300 - t=2.5	35.63	1.89
48	FE	5500	2960	38.3	600	ST	300×300 - t=2.5	39.10	2.06
49	FE	6000	2960	41.8	600	ST	300×300 - t=2.5	42.68	2.23
50	FE	6500	2960	45.2	600	ST	300×300 - t=2.5	46.15	2.40
51	FE	7000	2960	48.7	600	ST	300×300 - t=2.5	49.72	2.57
52	FE	7500	2960	52.1	600	ST	300×300 - t=2.5	53.19	2.74
53	FE	8000	2960	55.5	600	ST	300×300 - t=2.5	56.67	2.91
54	FE	9000	2960	62.4	600	ST	300×300 - t=2.5	63.71	3.24
55	T	1250	720	0.5	400	CT	∅ 250 - t=2.5	0.54	2.29
56	T	3000	1600	6.0	600	CT	∅ 250 - t=2.5	6.24	2.25
57	T	3500	1600	7.0	600	CT	∅ 250 - t=2.5	7.28	2.56
58	T	4000	1600	8.0	600	CT	∅ 250 - t=2.5	8.32	2.88
59	T	4000	1800	10.0	600	CT	∅ 250 - t=2.5	10.36	2.56
60	T	4800	2780	30.0	600	C	∅ 250 - t=2.5	30.66	1.94
61	FE	2250	1950	6.8	500	ST	300×300 - t=2	7.02	1.41
62	FE	2750	1950	8.3	500	ST	300×300 - t=2	8.56	1.67
63	FE	3250	1950	9.8	500	ST	300×300 - t=2	10.11	1.92
64	FE	3750	1950	11.3	500	ST	300×300 - t=2	11.66	2.18
65	FE	4250	1950	12.7	500	ST	300×300 - t=3	13.11	2.44
66	FE	4500	1950	13.5	500	ST	300×300 - t=3	13.93	2.56
67	FE	4750	1950	14.2	500	ST	300×300 - t=3	14.66	2.69
68	FE	5000	1950	15.0	500	ST	300×300 - t=3	15.48	2.82
69	FE	2250	2300	9.5	500	ST	300×300 - t=3	9.76	1.20
70	FE	3250	2300	13.6	500	ST	300×300 - t=3	13.97	1.63
71	FE	4250	2300	17.8	500	ST	300×300 - t=3	18.28	2.07
72	FE	4750	2300	19.8	500	ST	300×300 - t=3	20.34	2.28
73	FE	8500	3200	72.0	500	CT	∅ 300 - t=3	73.34	2.81
74	FE	11000	3200	92.0	500	CT	∅ 300 - t=3	93.74	3.59
75	FE	12000	3200	100.0	500	CT	∅ 300 - t=3	101.89	3.91
76	FE	5910	2000	16.0	500	ST	250×250 - t=3	16.58	3.21
77	FE	5410	2300	19.0	500	ST	250×250 - t=3	19.61	2.57
78	FE	6660	2300	24.3	500	ST	250×250 - t=3	25.06	3.11

79	FE	6140	2450	25.1	500	ST	250×250 - t=3	25.84	2.71
80	FE	8390	2450	35.9	500	ST	250×250 - t=3	36.91	3.63
81	FE	5470	2626	25.1	500	ST	300×300 - t=3	25.81	2.27
82	FE	6970	2626	33.2	500	ST	300×300 - t=3	34.10	2.84
83	FE	8470	2626	41.3	500	ST	300×300 - t=3	42.40	3.42
84	FE	6010	2826	30.0	500	ST	300×300 - t=3	30.84	2.30
85	FE	7490	2826	40.0	500	ST	300×300 - t=3	41.04	2.83
86	FE	9210	2826	50.0	500	ST	300×300 - t=3	51.28	3.44
87	FE	10790	2826	60.0	500	ST	300×300 - t=3	61.50	4.00
88	FE	8330	3000	50.0	500	ST	300×300 - t=3	51.23	2.94
89	FE	9750	3000	60.0	500	ST	300×300 - t=3	61.44	3.42
90	FE	11170	3000	70.0	500	ST	300×300 - t=3	71.65	3.89
91	FE	12350	3000	78.5	500	ST	300×300 - t=3	80.33	4.28
92	FE	11810	3500	100.0	500	ST	300×300 - t=3	102.04	3.52
93	T	5380	2300	21.6	600	CT	∅ 250 - t=3	22.21	2.60
94	T	2400	2450	10.4	600	CT	∅ 250 - t=3	10.69	1.22
95	T	3400	2450	15.2	600	CT	∅ 250 - t=3	15.61	1.63
96	T	4400	2450	19.9	600	CT	∅ 250 - t=3	20.43	2.04
97	T	5400	2450	24.6	600	CT	∅ 250 - t=3	25.25	2.45
98	T	3970	2626	20.3	600	CT	∅ 250 - t=3	20.81	1.74
99	T	4970	2626	25.7	600	CT	∅ 250 - t=3	26.34	2.12
100	T	6470	2626	33.8	600	CT	∅ 250 - t=3	34.64	2.69
101	T	5090	2826	30.1	600	ST	250×250 - t=3	30.81	2.01
102	T	6570	2826	39.4	600	ST	250×250 - t=3	40.32	2.54
103	T	8290	2826	50.2	600	ST	300×300 - t=3	51.36	3.15
104	T	9870	2826	60.1	600	ST	300×300 - t=3	61.48	3.70
105	T	6000	3000	40.4	600	ST	300×300 - t=3	41.29	2.20
106	T	7391	3000	50.3	600	ST	300×300 - t=3	51.39	2.66
107	T	8820	3000	60.3	600	ST	300×300 - t=3	61.61	3.14
108	T	10240	3000	70.7	600	ST	300×300 - t=3	72.22	3.61
109	T	11420	3000	79.1	600	ST	300×300 - t=3	80.79	4.01
110	FE	2250	3300	17.1	1050	ST	300×300 - t=3	17.47	1.00

5-leg vessels

#	Vessel type*	H_{wall} [mm]	D [mm]	C [m^3]	H_{leg} [mm]	Leg type**	Leg cross-section	Mass [t]	λ [-]
1	T	2250	2100	7.80	625	ST	300×300 - t=2.5	8.03	1.37
2	T	3000	2100	10.4	625	ST	300×300 - t=2.5	10.71	1.73
3	T	3750	2100	13.0	625	ST	300×300 - t=2.5	13.39	2.08
4	T	2750	2230	10.8	625	ST	300×300 - t=2.5	11.10	1.51
5	T	3000	2230	11.8	625	ST	300×300 - t=2.5	12.13	1.63
6	T	4000	2230	15.7	625	ST	300×300 - t=2.5	16.14	2.07
7	T	5500	2230	21.6	625	ST	300×300 - t=2.5	22.20	2.75
8	T	2250	2420	10.5	625	ST	300×300 - t=2.5	10.77	1.19
9	T	2750	2420	12.8	625	ST	300×300 - t=2.5	13.13	1.39
10	T	3500	2420	16.2	625	ST	300×300 - t=2.5	16.62	1.70

* Vessel type, where T: storage tank; FE: fermenter.

** Leg cross-section type, where S: squared; C: circular; ST: squared tapered; CT: circular tapered.

Table 3. Median (e^{μ}) and dispersion (σ) of the fitting lognormal cumulative distributions and relative coefficient of determination R^2 for the different groups and limit states.

#	e^{μ}_{uplift} [g]	σ_{uplift} [g]	R^2_{uplift} [-]	$e^{\mu}_{sliding}$ [g]	$\sigma_{sliding}$ [g]	$R^2_{sliding}$ [-]	$e^{\mu}_{collapse}$ [g]	$\sigma_{collapse}$ [g]	$R^2_{collapse}$ [-]
3-leg vessels									
1	0.1193	0.2067	0.97	0.1193	0.2067	0.93	0.3763	0.4736	0.86
2	0.1234	0.2475	0.91	0.1234	0.2475	0.89	0.4047	0.3053	0.89
3	0.1115	0.1762	0.91	0.1115	0.1762	0.88	0.3844	0.6608	0.87
4	0.1129	0.2020	0.98	0.1131	0.2054	0.88	0.3922	0.7588	0.85
5	0.1155	0.2373	0.90	0.1158	0.2359	0.90	0.4015	0.2906	0.87
6	0.1166	0.2518	0.92	0.1172	0.2541	0.92	0.3604	0.4459	0.86
7	0.1268	0.3090	0.92	0.1272	0.3080	0.93	0.4379	0.2473	0.88
8	0.1187	0.2083	0.95	0.1315	0.2184	0.92	0.4117	0.2533	0.87
9	0.1328	0.2489	0.89	0.1533	0.2499	0.90	0.4187	0.2502	0.88
10	0.1194	0.1817	0.93	0.1369	0.2208	0.89	0.4115	0.2195	0.86
11	0.1230	0.2290	0.93	0.1370	0.2201	0.92	0.3899	0.2623	0.89
12	0.1078	0.1429	0.89	0.1168	0.1776	0.90	0.4092	0.2132	0.88
13	0.1035	0.0571	0.90	0.1108	0.1229	0.92	0.4258	0.2613	0.88
14	0.1384	0.2259	0.93	0.1523	0.2212	0.88	0.4104	0.2519	0.85
15	0.1227	0.1808	0.90	0.1380	0.2185	0.93	0.4101	0.2165	0.86
16	0.1154	0.1662	0.94	0.1304	0.1758	0.93	0.4195	0.2185	0.85
17	0.1390	0.2550	0.94	0.1514	0.2434	0.91	0.4122	0.2364	0.89
18	0.1228	0.2006	0.98	0.1393	0.2280	0.90	0.4083	0.2097	0.88
19	0.1125	0.1609	0.89	0.1289	0.1897	0.90	0.4135	0.2313	0.88
20	0.1056	0.1140	0.95	0.1131	0.1644	0.91	0.4143	0.2550	0.87
4-leg vessels									
1	0.1529	0.3526	0.94	0.1585	0.3766	0.87	0.3808	0.5180	0.85
2	0.1572	0.4069	0.91	0.1669	0.4042	0.89	0.4290	0.2679	0.86
3	0.1525	0.2566	0.95	0.1702	0.2746	0.90	0.4294	0.2480	0.87
4	0.1363	0.2584	0.91	0.1601	0.2471	0.91	0.4232	0.2615	0.90
5	0.1676	0.2876	0.96	0.1963	0.2499	0.89	0.4698	0.2246	0.88
6	0.1418	0.2822	0.92	0.1709	0.2743	0.92	0.4625	0.2421	0.87
7	0.1487	0.2781	0.96	0.1770	0.2504	0.90	0.4466	0.2327	0.87
8	0.1331	0.2566	0.96	0.1591	0.2321	0.90	0.4353	0.2454	0.85
9	0.1404	0.2258	0.93	0.1625	0.2340	0.91	0.4373	0.2475	0.86
10	0.1401	0.2551	0.88	0.1644	0.2482	0.93	0.4599	0.2271	0.90
11	0.1404	0.2558	0.90	0.1652	0.2494	0.88	0.4775	0.2355	0.88
12	0.1212	0.1956	0.88	0.1374	0.2274	0.88	0.4473	0.2377	0.87
13	0.1046	0.0880	0.94	0.1292	0.1816	0.91	0.4319	0.2865	0.89
14	0.1205	0.1988	0.97	0.1374	0.2274	0.91	0.4413	0.2328	0.87
15	0.1113	0.1805	0.89	0.1227	0.1912	0.92	0.4453	0.2708	0.87
16	0.1089	0.1415	0.95	0.1209	0.1850	0.90	0.2094	0.2370	0.87
17	0.1059	0.1198	0.91	0.1106	0.1907	0.93	0.1036	0.2673	0.87
18	0.1544	0.4461	0.89	0.1572	0.4664	0.89	0.4061	0.3613	0.85
19	0.1481	0.2972	0.93	0.1570	0.3245	0.93	0.3772	0.2777	0.88
20	0.1268	0.2229	0.91	0.1507	0.2338	0.92	0.3285	0.2923	0.88
21	0.1284	0.2401	0.97	0.1349	0.2207	0.92	0.3746	0.2792	0.89
22	0.1429	0.2710	0.88	0.1628	0.2519	0.93	0.4135	0.2676	0.85
23	0.1421	0.2235	0.93	0.1638	0.2428	0.92	0.4232	0.2606	0.88
24	0.1178	0.1587	0.89	0.1392	0.2209	0.88	0.3703	0.2362	0.90
25	0.1381	0.2434	0.97	0.1631	0.2379	0.90	0.4637	0.2258	0.88
26	0.1177	0.2056	0.96	0.1441	0.2575	0.90	0.4288	0.1826	0.89
27	0.1229	0.2102	0.95	0.1475	0.2165	0.92	0.4468	0.2403	0.86
28	0.1138	0.1856	0.97	0.1381	0.2357	0.87	0.4365	0.2295	0.85
29	0.1050	0.1085	0.94	0.1304	0.2329	0.89	0.3318	0.2286	0.90
30	0.1168	0.1751	0.98	0.1228	0.1855	0.88	0.2738	0.3384	0.87

31	0.1574	0.3874	0.94	0.1775	0.3822	0.91	0.4491	0.2264	0.89
32	0.1253	0.1807	0.95	0.1466	0.2524	0.89	0.3837	0.2471	0.90
33	0.1660	0.3131	0.88	0.1920	0.2657	0.90	0.4765	0.2143	0.89
34	0.1195	0.1713	0.94	0.1378	0.2502	0.87	0.4180	0.2106	0.86
35	0.1687	0.3164	0.93	0.1974	0.3134	0.88	0.4894	0.2628	0.90
36	0.1476	0.2181	0.96	0.1745	0.2426	0.91	0.4662	0.2381	0.85
37	0.1345	0.2431	0.93	0.1559	0.2391	0.89	0.4404	0.2648	0.86
38	0.1238	0.2299	0.91	0.1385	0.2569	0.92	0.4352	0.2387	0.88
39	0.1165	0.1759	0.95	0.1319	0.2062	0.88	0.4151	0.2710	0.90
40	0.1102	0.1577	0.96	0.1321	0.1977	0.89	0.4229	0.2574	0.85
41	0.1150	0.1672	0.89	0.1266	0.2127	0.88	0.4394	0.2249	0.90
42	0.1179	0.1876	0.90	0.1332	0.2246	0.88	0.4468	0.1984	0.87
43	0.1301	0.2400	0.91	0.1651	0.2628	0.87	0.4608	0.2227	0.88
44	0.1264	0.2382	0.90	0.1418	0.2660	0.88	0.4620	0.2404	0.86
45	0.1221	0.2250	0.96	0.1384	0.2287	0.87	0.4491	0.2239	0.86
46	0.1173	0.2081	0.88	0.1290	0.2397	0.92	0.3306	0.2241	0.89
47	0.1152	0.2010	0.91	0.1296	0.2472	0.91	0.1812	0.2148	0.89
48	0.1142	0.2175	0.96	0.1208	0.2287	0.92	0.1253	0.2411	0.88
49	0.1082	0.1201	0.95	0.1109	0.1405	0.91	0.1109	0.1798	0.87
50	0.1065	0.1250	0.97	0.1102	0.1440	0.90	0.1158	0.2216	0.89
51	0.1009	0.0370	0.92	0.1070	0.1107	0.87	0.1110	0.1987	0.86
52	0.1027	0.0724	0.92	0.1062	0.1185	0.91	0.1089	0.2352	0.86
53	0.1049	0.0880	0.97	0.1116	0.1541	0.91	0.1215	0.2939	0.87
54	0.1051	0.0992	0.89	0.1114	0.1309	0.89	0.1236	0.2821	0.86
55	0.1369	0.3102	0.92	0.1369	0.3102	0.87	0.2056	0.6047	0.87
56	0.1273	0.2259	0.95	0.1497	0.2009	0.88	0.3912	0.2556	0.86
57	0.1181	0.1619	0.91	0.1366	0.1889	0.89	0.3844	0.2537	0.87
58	0.1141	0.1446	0.92	0.1397	0.1941	0.92	0.3534	0.2456	0.88
59	0.1160	0.1790	0.94	0.1323	0.2214	0.90	0.3767	0.2376	0.89
60	0.1150	0.2258	0.89	0.1268	0.2273	0.90	0.3572	0.2344	0.87
61	0.1497	0.2444	0.89	0.1772	0.2481	0.92	0.4543	0.2345	0.89
62	0.1359	0.2424	0.95	0.1686	0.2514	0.91	0.4525	0.2394	0.89
63	0.1292	0.2478	0.96	0.1543	0.2489	0.87	0.4407	0.1980	0.90
64	0.1215	0.2102	0.93	0.1388	0.2207	0.92	0.4354	0.2455	0.87
65	0.1206	0.1957	0.90	0.1389	0.2127	0.88	0.4188	0.1951	0.90
66	0.1132	0.1869	0.91	0.1340	0.2324	0.88	0.3897	0.2615	0.86
67	0.1104	0.1491	0.93	0.1298	0.1995	0.92	0.3976	0.2556	0.89
68	0.1116	0.1341	0.95	0.1332	0.2143	0.88	0.3852	0.2887	0.90
69	0.1568	0.3189	0.92	0.1932	0.2647	0.90	0.4879	0.2136	0.88
70	0.1348	0.2239	0.98	0.1562	0.2712	0.90	0.4506	0.1910	0.89
71	0.1178	0.1915	0.90	0.1335	0.2269	0.93	0.4332	0.2511	0.89
72	0.1108	0.1442	0.90	0.1332	0.2050	0.92	0.4273	0.2645	0.86
73	0.1059	0.1139	0.95	0.1063	0.1133	0.91	0.1248	0.3254	0.85
74	0.1070	0.1080	0.89	0.1132	0.1737	0.88	0.1270	0.2783	0.87
75	0.1122	0.1447	0.90	0.1206	0.1952	0.89	0.1304	0.2648	0.89
76	0.1077	0.1290	0.93	0.1419	0.2069	0.92	0.3981	0.2574	0.85
77	0.1101	0.1615	0.90	0.1341	0.2194	0.92	0.4293	0.2123	0.86
78	0.1052	0.1389	0.90	0.1340	0.1985	0.89	0.4252	0.3163	0.89
79	0.1097	0.1471	0.89	0.1255	0.2188	0.89	0.4221	0.2603	0.88
80	0.1043	0.0802	0.94	0.1332	0.2257	0.89	0.1270	0.2451	0.86
81	0.1126	0.1828	0.93	0.1266	0.2062	0.89	0.4348	0.2063	0.85
82	0.1053	0.0861	0.97	0.1282	0.2081	0.88	0.4173	0.2753	0.86
83	0.1033	0.0776	0.93	0.1410	0.2507	0.90	0.1434	0.2601	0.86
84	0.1111	0.1609	0.97	0.1249	0.1985	0.93	0.4509	0.2719	0.86
85	0.1054	0.1064	0.97	0.1248	0.2011	0.92	0.1901	0.2563	0.87
86	0.1066	0.1113	0.93	0.1308	0.2072	0.91	0.1290	0.2510	0.89
87	0.1036	0.0815	0.96	0.1224	0.2109	0.88	0.1252	0.2629	0.89
88	0.1034	0.0740	0.96	0.1162	0.1980	0.91	0.1138	0.2680	0.86
89	0.1062	0.1215	0.92	0.1219	0.1987	0.91	0.1547	0.2255	0.88

90	0.1033	0.0810	0.94	0.1199	0.1839	0.88	0.1524	0.2629	0.88
91	0.1094	0.1281	0.89	0.1300	0.2441	0.90	0.1709	0.2962	0.87
92	0.1088	0.1433	0.97	0.1107	0.1466	0.89	0.1273	0.2814	0.88
93	0.1088	0.1412	0.90	0.1282	0.1982	0.87	0.3896	0.2611	0.88
94	0.1525	0.2448	0.90	0.1806	0.2433	0.91	0.4788	0.2315	0.86
95	0.1318	0.2399	0.91	0.1535	0.2693	0.93	0.4424	0.2554	0.88
96	0.1209	0.2101	0.91	0.1335	0.1799	0.89	0.4358	0.2166	0.88
97	0.1125	0.1732	0.88	0.1320	0.2103	0.91	0.2772	0.2150	0.88
98	0.1185	0.2095	0.94	0.1419	0.2447	0.89	0.4328	0.2613	0.90
99	0.1126	0.2052	0.91	0.1287	0.2370	0.87	0.2369	0.2362	0.88
100	0.1059	0.0907	0.94	0.1104	0.1061	0.88	0.1196	0.1658	0.90
101	0.1127	0.1940	0.98	0.1156	0.2107	0.92	0.1190	0.2324	0.86
102	0.1055	0.0969	0.94	0.1055	0.0969	0.92	0.1128	0.1996	0.86
103	0.1039	0.0907	0.92	0.1174	0.2169	0.89	0.1224	0.3134	0.90
104	0.1046	0.0882	0.98	0.1157	0.1659	0.89	0.1226	0.2709	0.89
105	0.1088	0.1432	0.96	0.1116	0.1538	0.91	0.1126	0.1883	0.87
106	0.1034	0.0689	0.97	0.1056	0.0821	0.90	0.1118	0.1835	0.88
107	0.1048	0.0975	0.92	0.1134	0.1890	0.89	0.1197	0.2570	0.87
108	0.1028	0.0632	0.92	0.1133	0.1518	0.87	0.1209	0.2678	0.89
109	0.1040	0.0819	0.95	0.1180	0.1672	0.89	0.1305	0.2883	0.86
110	0.1479	0.2326	0.98	0.1742	0.2713	0.92	0.4092	0.2229	0.89
5-leg vessels									
1	0.1623	0.3044	0.98	0.1987	0.2610	0.90	0.5172	0.2340	0.89
2	0.1356	0.2229	0.92	0.1733	0.2175	0.90	0.4848	0.2733	0.87
3	0.1170	0.1797	0.94	0.1582	0.2370	0.88	0.4576	0.2560	0.90
4	0.1475	0.2615	0.96	0.1839	0.2596	0.91	0.5155	0.2414	0.87
5	0.1326	0.2223	0.89	0.1694	0.2317	0.89	0.4982	0.2596	0.87
6	0.1249	0.2294	0.96	0.1488	0.2379	0.93	0.4772	0.2280	0.88
7	0.1073	0.1110	0.97	0.1447	0.2139	0.90	0.4760	0.2638	0.86
8	0.1613	0.2982	0.92	0.2048	0.2673	0.91	0.5326	0.2554	0.89
9	0.1453	0.2865	0.95	0.1882	0.2555	0.91	0.5179	0.2333	0.89
10	0.1261	0.2501	0.97	0.1601	0.2851	0.88	0.5034	0.2350	0.89

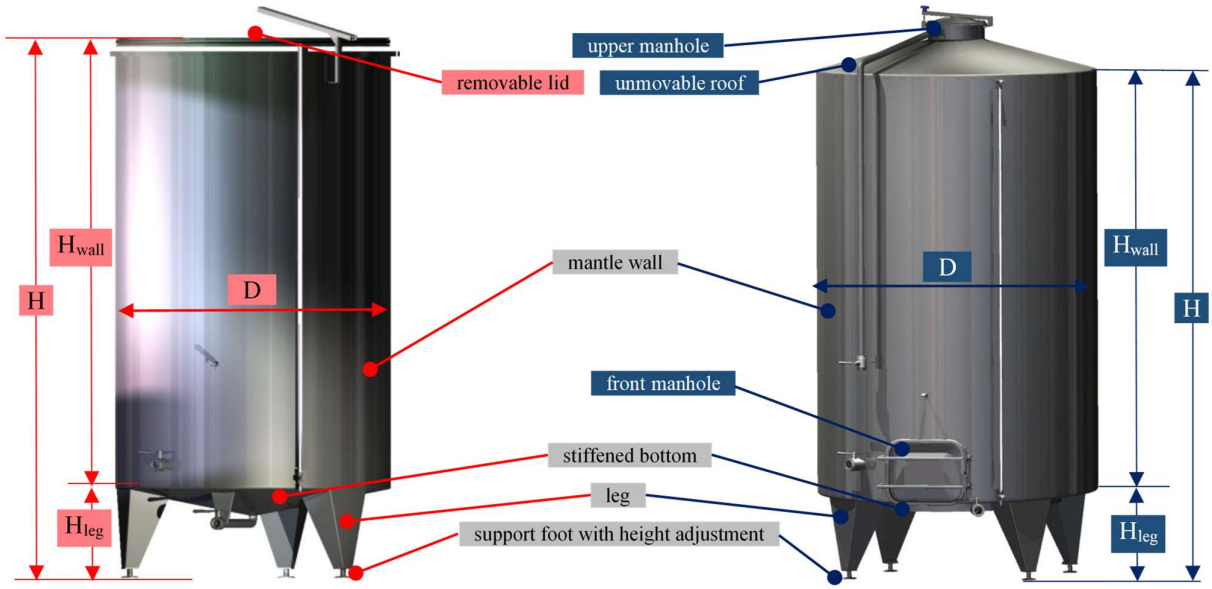

Figure 1. Details of the typical vessels used in wine-making industry. Images adapted from [27]. (a) Tank; (b) Fermenter.

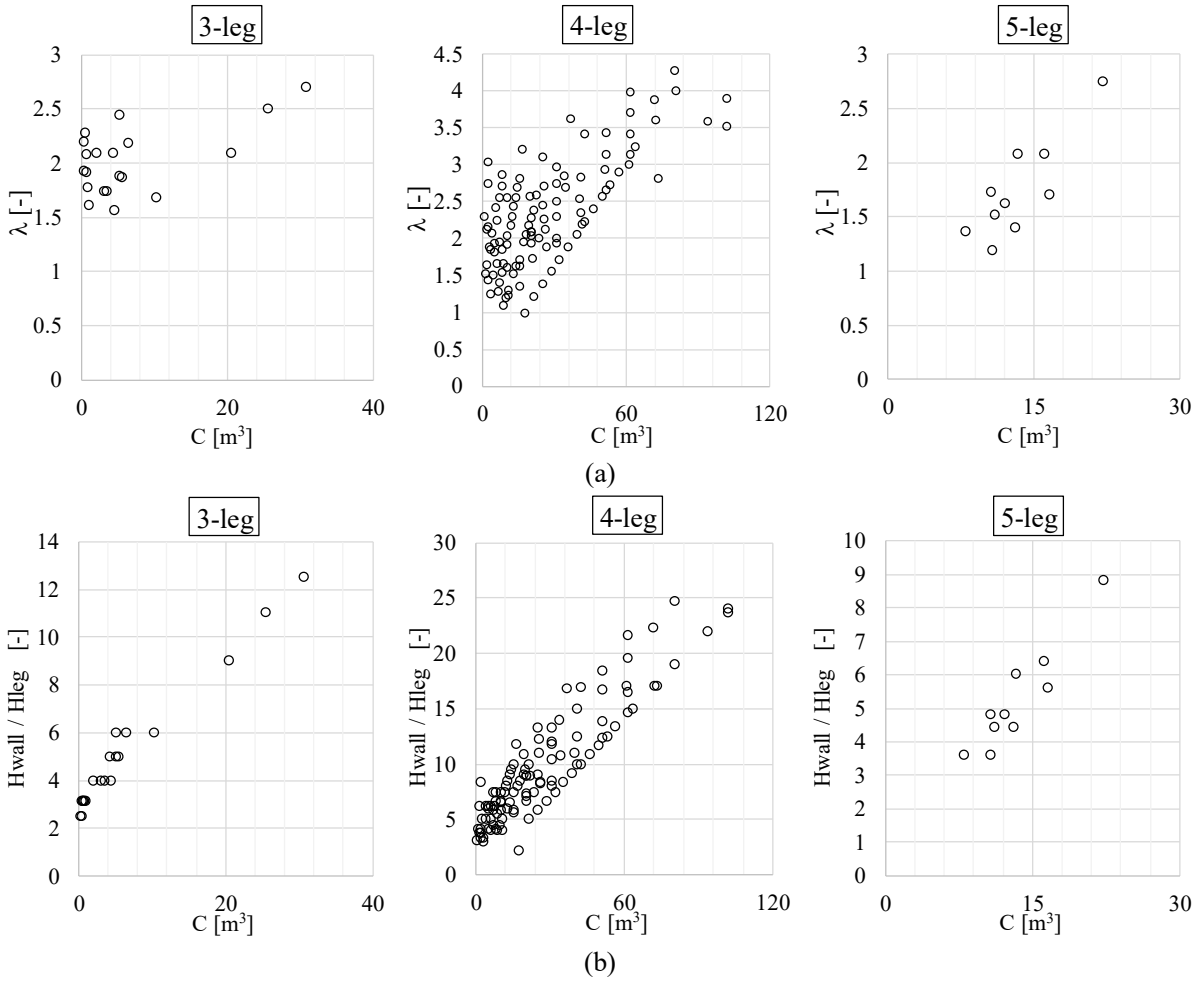

Figure 2. Distributions of the main geometrical properties of vessels as a function of the capacity C. (a) λ ratio (where $\lambda = H / D$). (b) H_{wall} / H_{leg} ratio.

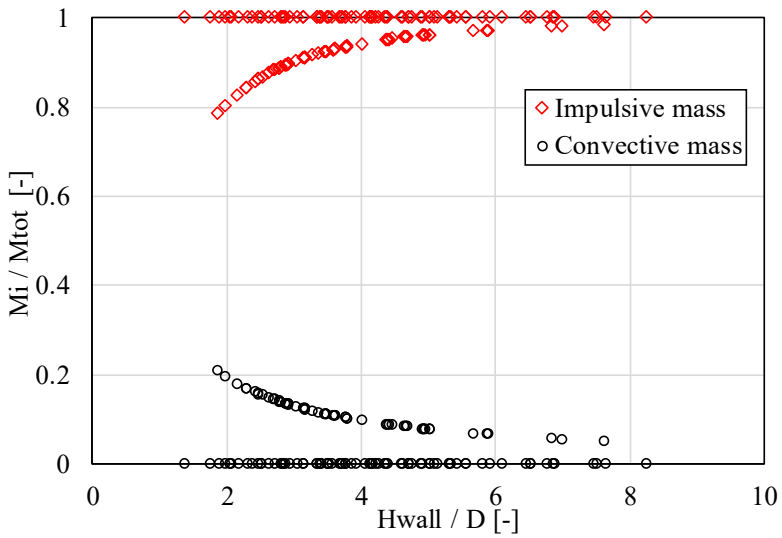

Figure 3. Impulsive and convective mass fraction as function of the ratio *Hwall / D*.

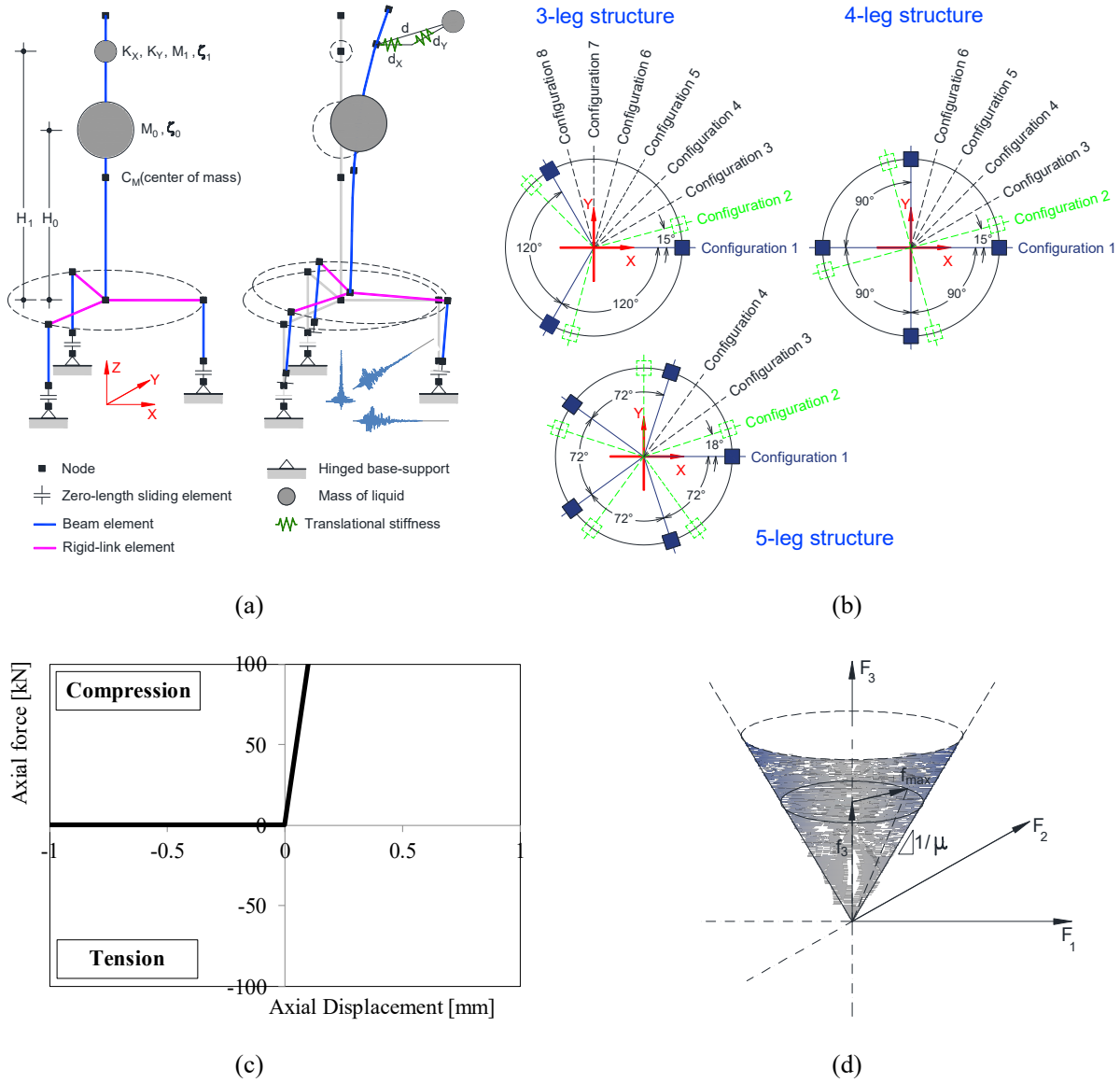

Figure 4. Finite element model adopted for the dynamic seismic analyses of the vessels. (a) Views of the model in undeformed and in deformed shape. (b) Schemes of the various configurations considered during time-history analyses for each group of structures (i.e. 3, 4 and 5-leg type). (c) Axial (direction 3) behaviour of the zero-length element at the base. (d) 3D coupled behavior among the three local directions 1, 2 and 3 of the zero-length element ate the base.

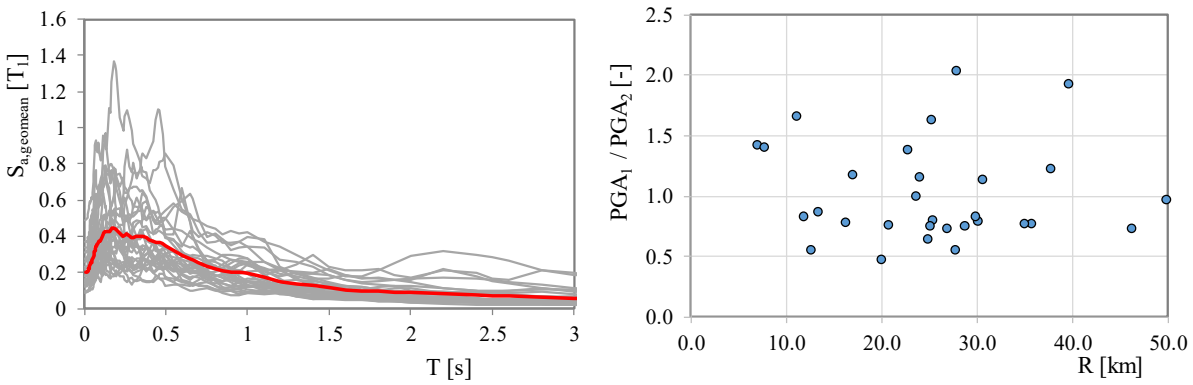

(a) (b)

Figure 5. Main characteristics of the ground motions adopted in the present paper. (a) Horizontal geometric mean (geomean) elastic acceleration response spectra for 5% damping ratio of ground motions (grey lines) and average of the 30 geomean acceleration response spectra (the red line). (b) PGA_1/PGA_2 for the two horizontal components as a function of R (closest distance from the fault rupture).

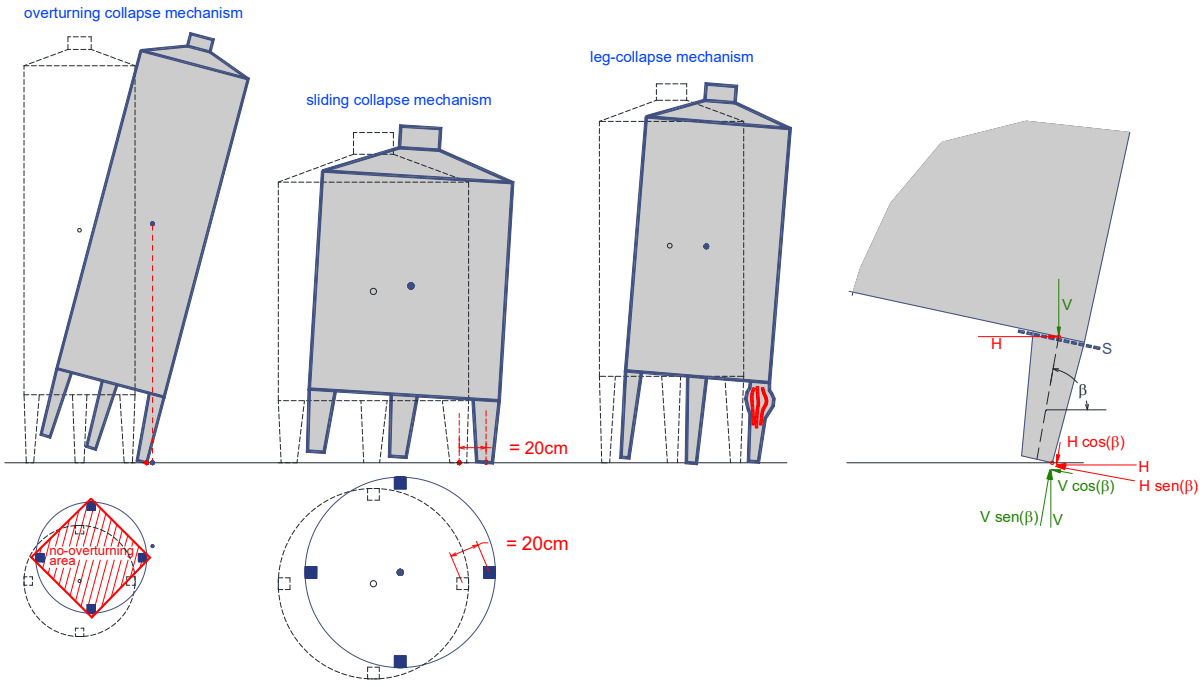

(a) (b)

Figure 6. Collapse mechanisms (a) considered in the work: tank overturning, tank excessive sliding or failure of legs and (b) Decomposition of the horizontal and vertical force on a leg for the determination of second order effects and localization of the verification cross-section S.

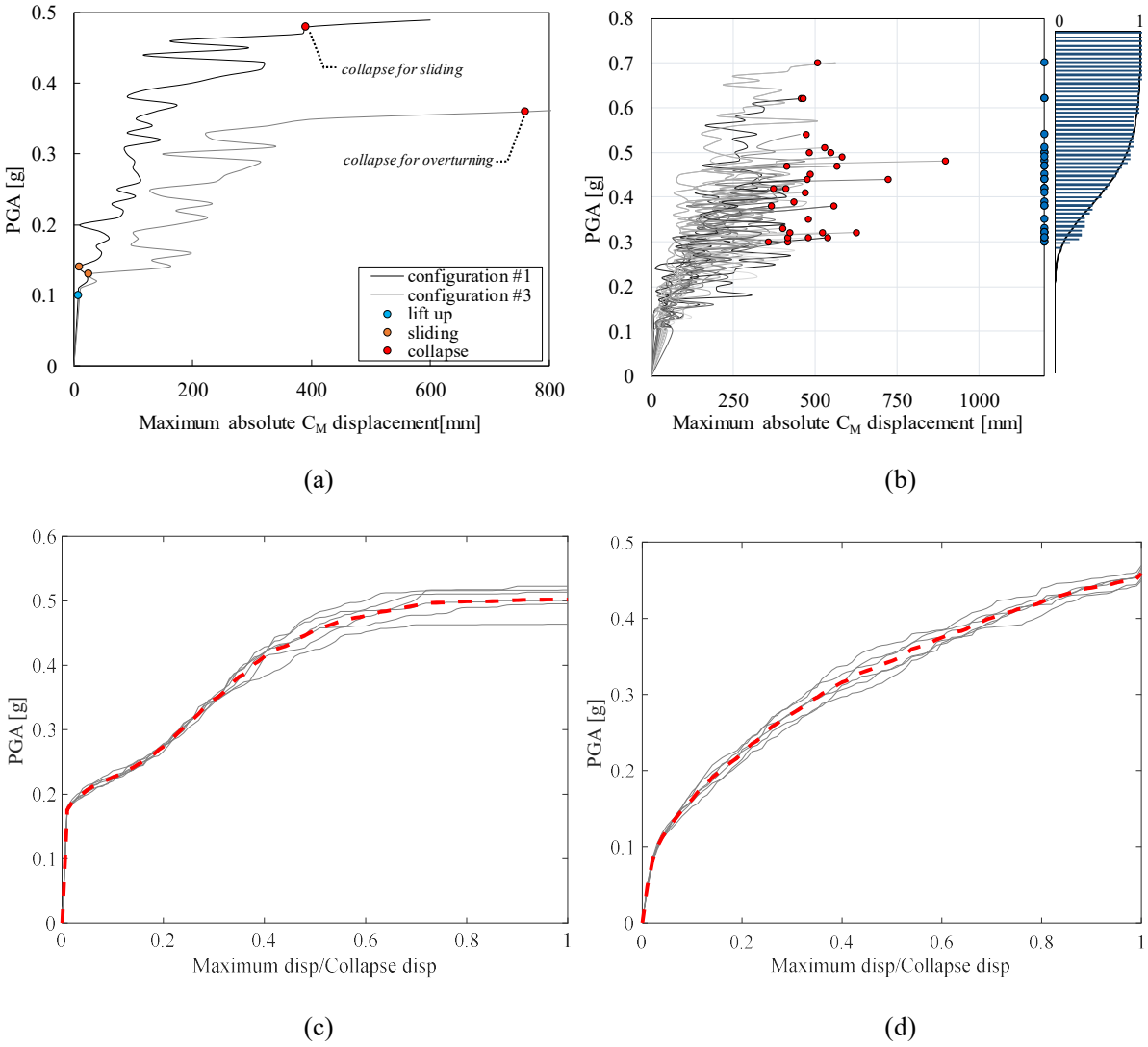

Figure 7. Features of the IDA curves. (a) Comparison between IDA curve emerging from two different configurations (#1 and #3) for a 4-leg tank #17 subjected to same seismic input. (b) Different IDA curves provided from a tank in one specific configuration (red circles identified the collapse). Example of generation of empirical and best-fitting collapse fragilities starting from the collapse PGA values (blue circles). Example of IDA curves variability for a 3-leg and 4-leg structure respectively (c) and (d).

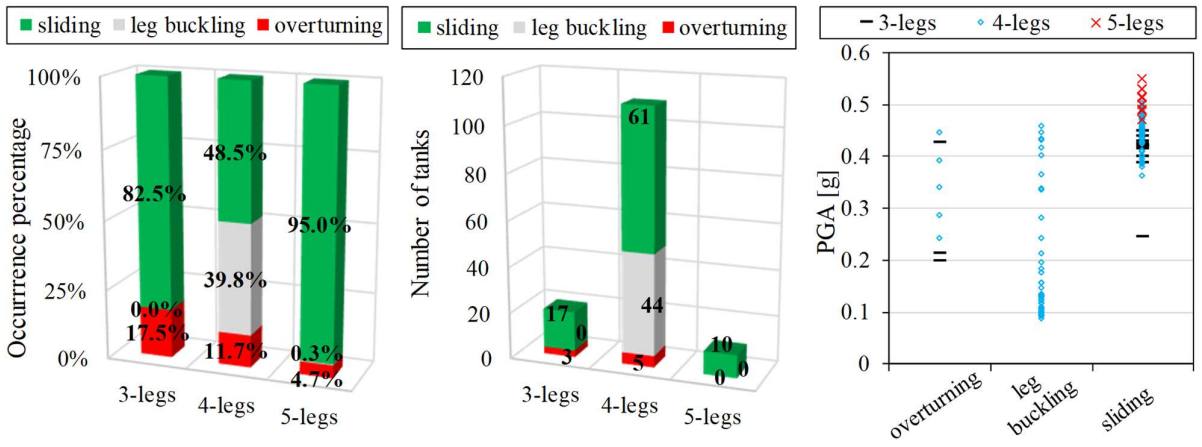

(a) (b) (c)

Figure 8. Summary of the main outcomes at the tanks collapse state provided by IDA. (a) Occurrence percentage of the various collapse mechanisms from the whole IDAs set. (b) Most frequent collapse causes. (c) Median collapse PGA values computed for each tank by considering the whole outcomes set coming from the 30 time histories performed for *n* configurations (where *n* is equal to 8, 6 and 4 respectively for the 3-, 4- and 5-leg vessels).

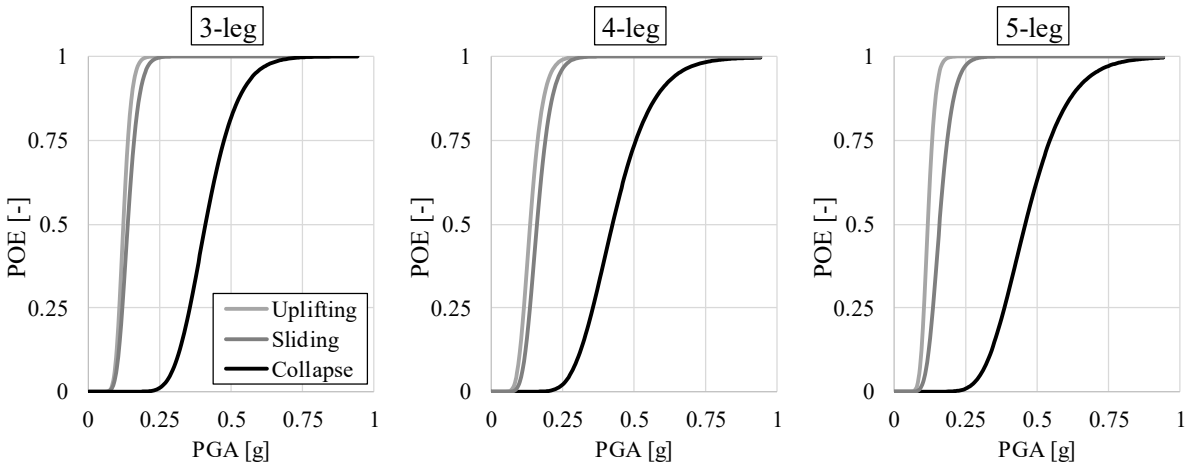

(a) (b) (c)

Figure 9. Fragility curves of (a) 3-leg tank #15, (b) 4-leg tank # 4 and 5-leg tank #3.

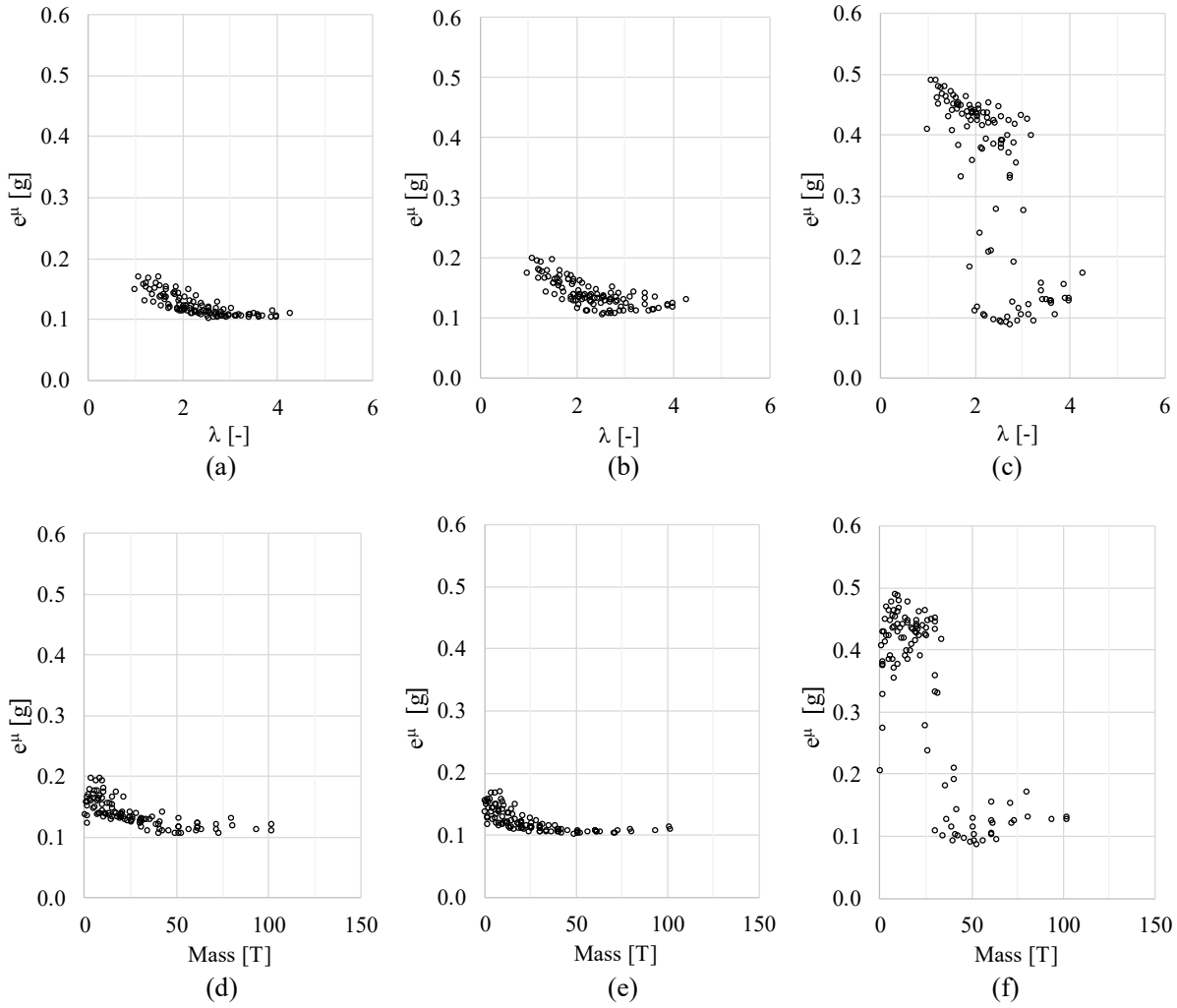

Figure 10. Distribution of 4-leg tanks fragility median: as a function of λ for (a) uplifting, (b) sliding and (c) collapse state; as a function of the total mass M again for (d) uplifting, (e) sliding and (f) collapse state.

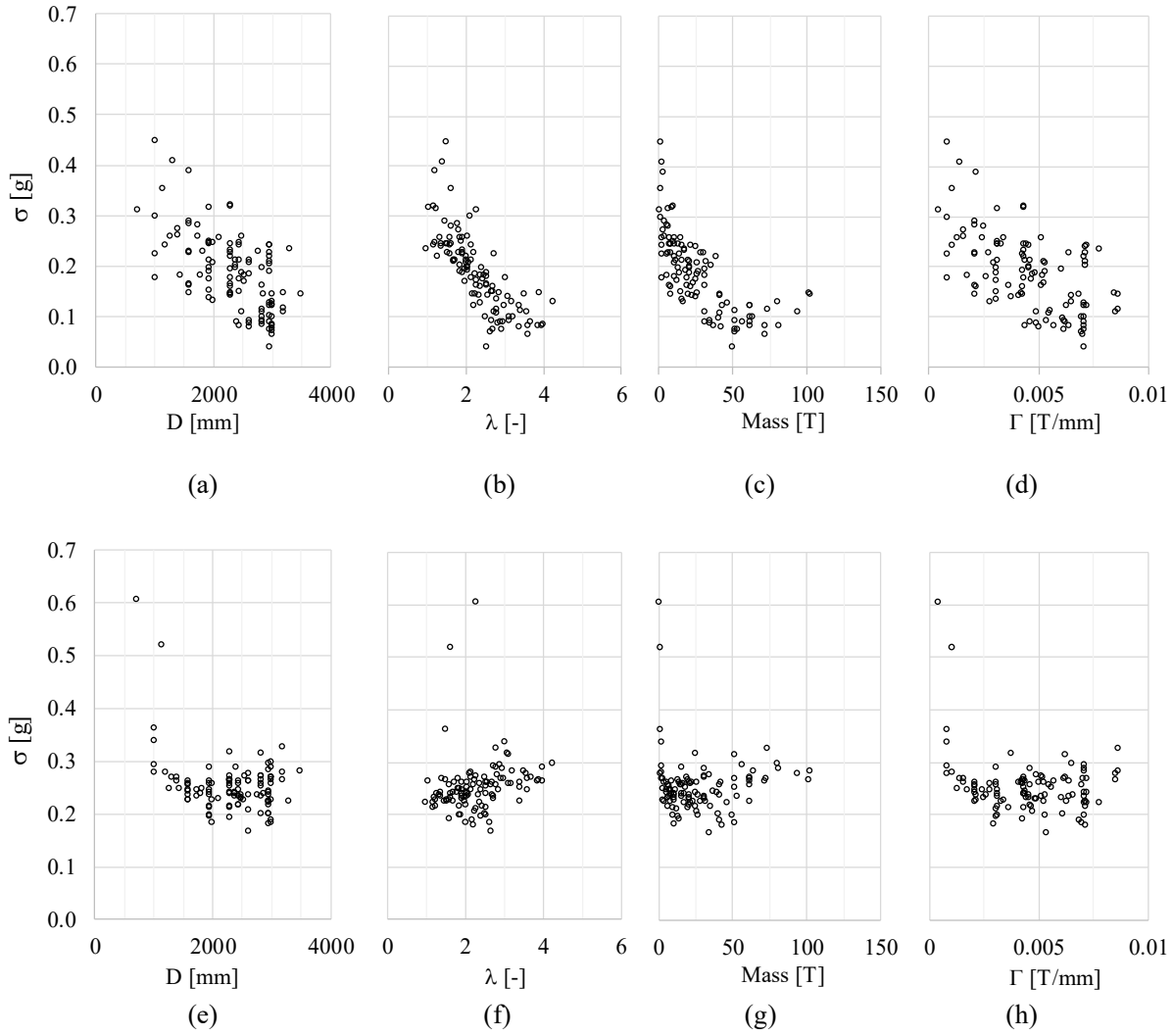

Figure 11. Distribution of 4-leg tanks fragility dispersion at the uplifting activation state as a function (a) diameter, (b) aspect ratio λ, (c) total mass M and (d) ratio $\Gamma=M/H_{wall}$ and at collapse state (e)-(h).

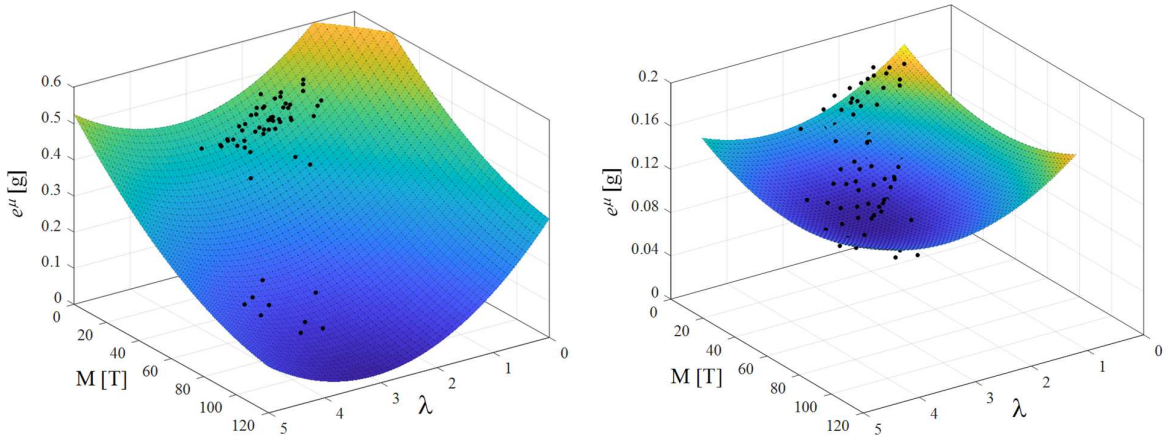

(a) (b)

Figure 12. Second order fitting RS of fragility median for (a) collapse and (b) uplift limit states for 4-leg tanks group.

Table 1. Main characteristics of the vessels considered in the present paper.

3-leg vessels

Id.	Vessel type*	H_{wall} [mm]	D [mm]	C [kl]	H_{leg} [mm]	Leg type**	Leg cross-section	λ (H/D)
1	T	1000	636	0.3	400	S	250×250 - t=2	2.20
2	T	1000	724	0.4	400	S	250×250 - t=2	1.93
3	T	1250	724	0.5	400	S	250×250 - t=2	2.28
4	T	1250	794	0.6	400	S	250×250 - t=2	2.08
5	T	1250	858	0.7	400	S	250×250 - t=2	1.92
6	T	1250	928	0.8	400	S	250×250 - t=2	1.78
7	T	1250	1020	1.0	400	S	250×250 - t=2	1.62
8	T	2000	1194	2.0	500	CT	∅ 300 - t=2.5	2.09
9	T	2000	1430	3.0	500	CT	∅ 300 - t=2.5	1.75
10	T	2500	1593	5.0	500	C	∅ 300 - t=2.5	1.88
11	T	3000	2070	10.0	500	C	∅ 300 - t=2.5	1.69
12	T	4500	2388	20.0	500	S	300×300 - t=2.5	2.09
13	T	6250	2500	30.0	500	S	300×300 - t=2.5	2.70
14	FE	2000	1430	3.4	500	S	300×300 - t=2.5	1.75
15	FE	2500	1430	4.2	500	S	300×300 - t=2.5	2.10
16	FE	3000	1430	5.0	500	S	300×300 - t=2.5	2.45
17	FE	2000	1600	4.3	500	S	300×300 - t=2.5	1.56
18	FE	2500	1600	5.3	500	S	300×300 - t=2.5	1.88
19	FE	3000	1600	6.3	500	S	300×300 - t=2.5	2.19
20	FE	5500	2400	25.0	500	S	300×300 - t=2.5	2.50

4-leg vessels

Id.	Vessel type	H_{wall} [mm]	D [mm]	C [kl]	H_{leg} [mm]	Leg type	Leg cross-section	λ (H/D)
1	T	1500	1150	1.5	400	ST	250×250 - t=2.5	1.65
2	T	1500	1320	2.0	400	ST	250×250 - t=2.5	1.44
3	T	2000	1274	2.5	400	ST	250×250 - t=2.5	1.88
4	T	2500	1400	3.8	400	ST	250×250 - t=2.5	2.07
5	T	2000	1592	4.0	400	ST	250×250 - t=2.5	1.51
6	T	2500	1592	5.0	400	ST	250×250 - t=2.5	1.82
7	T	2500	1740	6.0	400	ST	250×250 - t=2.5	1.67
8	T	3000	1740	7.0	400	ST	250×250 - t=2.5	1.95
9	T	3000	1840	8.0	400	ST	250×250 - t=2.5	1.85
10	T	3000	2100	10.0	400	ST	250×250 - t=2.5	1.62
11	T	3000	2500	15.0	400	ST	250×250 - t=2.5	1.36
12	FE	4480	2388	20.0	500	C	∅ 300 - t=2.5	2.09
13	FE	6650	2400	30.0	500	C	∅ 300 - t=2.5	2.98
14	T	4480	2388	20.0	500	CT	∅ 300 - t=2.5	2.09
15	T	5900	2547	30.0	500	CT	∅ 300 - t=2.5	2.51
16	T	6250	2866	40.0	500	CT	∅ 300 - t=2.5	2.36
17	T	8500	3000	60.0	500	CT	∅ 300 - t=2.5	3.00
18	FE	1250	1020	1.0	300	ST	300×300 - t=2.5	1.52
19	FE	1870	1020	1.5	300	ST	300×300 - t=2.5	2.13
20	FE	2500	1020	2.0	300	ST	300×300 - t=2.5	2.75
21	FE	2000	1200	2.0	600	ST	300×300 - t=2.5	2.17
22	FE	2000	1400	3.0	600	ST	300×300 - t=2.5	1.86
23	FE	2500	1600	5.0	600	ST	300×300 - t=2.5	1.94
24	FE	3750	1600	7.7	600	ST	300×300 - t=2.5	2.72
25	FE	2500	2000	8.0	600	ST	300×300 - t=2.5	1.55
26	FE	3500	2000	10.0	600	ST	300×300 - t=2.5	2.05
27	FE	3500	2390	15.0	600	ST	300×300 - t=2.5	1.72
28	FE	4250	2500	20.0	600	ST	300×300 - t=2.5	1.94
29	FE	6250	2500	30.0	600	ST	300×300 - t=2.5	2.74
30	T	2500	1020	2.0	600	CT	∅ 300 - t=2.5	3.04

31	FE	1500	1600	3.1	500	ST	300×300 - t=2.5	1.25
32	FE	3000	1450	5.0	500	ST	300×300 - t=2.5	2.41
33	FE	2000	1950	6.1	500	ST	300×300 - t=2.5	1.28
34	FE	4000	1950	12.0	500	ST	300×300 - t=2.5	2.31
35	FE	2000	2300	8.5	500	ST	300×300 - t=2.5	1.09
36	FE	2500	2300	10.5	500	ST	300×300 - t=2.5	1.30
37	FE	3000	2300	12.6	500	ST	300×300 - t=2.5	1.52
38	FE	4000	2300	16.8	500	ST	300×300 - t=2.5	1.96
39	FE	4500	2300	18.9	500	ST	300×300 - t=2.5	2.17
40	FE	5000	2300	20.9	500	ST	300×300 - t=2.5	2.39
41	FE	4500	2540	23.1	600	ST	300×300 - t=2.5	2.01
42	FE	5000	2960	25.7	600	ST	300×300 - t=2.5	1.89
43	FE	3000	2960	21.1	600	ST	300×300 - t=2.5	1.22
44	FE	3500	2960	24.6	600	ST	300×300 - t=2.5	1.39
45	FE	4000	2960	28.0	600	ST	300×300 - t=2.5	1.55
46	FE	4500	2960	31.5	600	ST	300×300 - t=2.5	1.72
47	FE	5000	2960	34.9	600	ST	300×300 - t=2.5	1.89
48	FE	5500	2960	38.3	600	ST	300×300 - t=2.5	2.06
49	FE	6000	2960	41.8	600	ST	300×300 - t=2.5	2.23
50	FE	6500	2960	45.2	600	ST	300×300 - t=2.5	2.40
51	FE	7000	2960	48.7	600	ST	300×300 - t=2.5	2.57
52	FE	7500	2960	52.1	600	ST	300×300 - t=2.5	2.74
53	FE	8000	2960	55.5	600	ST	300×300 - t=2.5	2.91
54	FE	9000	2960	62.4	600	ST	300×300 - t=2.5	3.24
55	T	1250	720	0.5	400	CT	∅ 250 - t=2.5	2.29
56	T	3000	1600	6.0	600	CT	∅ 250 - t=2.5	2.25
57	T	3500	1600	7.0	600	CT	∅ 250 - t=2.5	2.56
58	T	4000	1600	8.0	600	CT	∅ 250 - t=2.5	2.88
59	T	4000	1800	10.0	600	CT	∅ 250 - t=2.5	2.56
60	T	4800	2780	30.0	600	C	∅ 250 - t=2.5	1.94
61	FE	2250	1950	6.8	500	ST	300×300 - t=2	1.41
62	FE	2750	1950	8.3	500	ST	300×300 - t=2	1.67
63	FE	3250	1950	9.8	500	ST	300×300 - t=2	1.92
64	FE	3750	1950	11.3	500	ST	300×300 - t=2	2.18
65	FE	4250	1950	12.7	500	ST	300×300 - t=3	2.44
66	FE	4500	1950	13.5	500	ST	300×300 - t=3	2.56
67	FE	4750	1950	14.2	500	ST	300×300 - t=3	2.69
68	FE	5000	1950	15.0	500	ST	300×300 - t=3	2.82
69	FE	2250	2300	9.5	500	ST	300×300 - t=3	1.20
70	FE	3250	2300	13.6	500	ST	300×300 - t=3	1.63
71	FE	4250	2300	17.8	500	ST	300×300 - t=3	2.07
72	FE	4750	2300	19.8	500	ST	300×300 - t=3	2.28
73	FE	8500	3200	72.0	500	CT	∅ 300 - t=3	2.81
74	FE	11000	3200	92.0	500	CT	∅ 300 - t=3	3.59
75	FE	12000	3200	100.0	500	CT	∅ 300 - t=3	3.91
76	FE	5910	2000	16.0	500	ST	250×250 - t=3	3.21
77	FE	5410	2300	19.0	500	ST	250×250 - t=3	2.57
78	FE	6660	2300	24.3	500	ST	250×250 - t=3	3.11
79	FE	6140	2450	25.1	500	ST	250×250 - t=3	2.71
80	FE	8390	2450	35.9	500	ST	250×250 - t=3	3.63
81	FE	5470	2626	25.1	500	ST	300×300 - t=3	2.27
82	FE	6970	2626	33.2	500	ST	300×300 - t=3	2.84
83	FE	8470	2626	41.3	500	ST	300×300 - t=3	3.42
84	FE	6010	2826	30.0	500	ST	300×300 - t=3	2.30
85	FE	7490	2826	40.0	500	ST	300×300 - t=3	2.83
86	FE	9210	2826	50.0	500	ST	300×300 - t=3	3.44
87	FE	10790	2826	60.0	500	ST	300×300 - t=3	4.00
88	FE	8330	3000	50.0	500	ST	300×300 - t=3	2.94
89	FE	9750	3000	60.0	500	ST	300×300 - t=3	3.42
90	FE	11170	3000	70.0	500	ST	300×300 - t=3	3.89

91	FE	12350	3000	78.5	500	ST	300×300 - t=3	4.28
92	FE	11810	3500	100.0	500	ST	300×300 - t=3	3.52
93	T	5380	2300	21.6	600	CT	∅ 250 - t=3	2.60
94	T	2400	2450	10.4	600	CT	∅ 250 - t=3	1.22
95	T	3400	2450	15.2	600	CT	∅ 250 - t=3	1.63
96	T	4400	2450	19.9	600	CT	∅ 250 - t=3	2.04
97	T	5400	2450	24.6	600	CT	∅ 250 - t=3	2.45
98	T	3970	2626	20.3	600	CT	∅ 250 - t=3	1.74
99	T	4970	2626	25.7	600	CT	∅ 250 - t=3	2.12
100	T	6470	2626	33.8	600	CT	∅ 250 - t=3	2.69
101	T	5090	2826	30.1	600	ST	250×250 - t=3	2.01
102	T	6570	2826	39.4	600	ST	250×250 - t=3	2.54
103	T	8290	2826	50.2	600	ST	300×300 - t=3	3.15
104	T	9870	2826	60.1	600	ST	300×300 - t=3	3.70
105	T	6000	3000	40.4	600	ST	300×300 - t=3	2.20
106	T	7391	3000	50.3	600	ST	300×300 - t=3	2.66
107	T	8820	3000	60.3	600	ST	300×300 - t=3	3.14
108	T	10240	3000	70.7	600	ST	300×300 - t=3	3.61
109	T	11420	3000	79.1	600	ST	300×300 - t=3	4.01
110	FE	2250	3300	17.1	1050	ST	300×300 - t=3	1.00

5-leg vessels

Id.	Vessel type	H_{wall} [mm]	D [mm]	C [kl]	H_{leg} [mm]	Leg type	Leg cross-section	λ (H/D)
1	T	2250	2100	7.80	625	ST	300×300 - t=2.5	1.37
2	T	3000	2100	10.4	625	ST	300×300 - t=2.5	1.73
3	T	3750	2100	13.0	625	ST	300×300 - t=2.5	2.08
4	T	2750	2230	10.8	625	ST	300×300 - t=2.5	1.51
5	T	3000	2230	11.8	625	ST	300×300 - t=2.5	1.63
6	T	4000	2230	15.7	625	ST	300×300 - t=2.5	2.07
7	T	5500	2230	21.6	625	ST	300×300 - t=2.5	2.75
8	T	2250	2420	10.5	625	ST	300×300 - t=2.5	1.19
9	T	2750	2420	12.8	625	ST	300×300 - t=2.5	1.39
10	T	3500	2420	16.2	625	ST	300×300 - t=2.5	1.70

* Vessel type where T: storage tank; FE: fermenter.

** Leg cross-section where S: squared; C: circular; ST: squared tapered; CT: circular tapered.

Table 2. Set of ground motions adopted in the IDA procedure.

No.	Event name	Station	M*	R** [km]	Mech.***	PGA_1 [g]	PGA_2 [g]	PGA_V [g]	PGV_1 [cm/s]	PGV_2 [cm/s]	PGA_1/PGA_2
1	San Fernando,1971	LA - Hollywood Stor FF	6.61	22.77	R	0.225	0.163	0.164	23.412	17.408	1.383
2	Imperial Valley-06,1979	Parachute Test Site	6.53	12.69	SS	0.113	0.206	0.162	6.103	11.182	0.548
3	Superstition Hills-02,1987	Brawley Airport	6.54	17.03	SS	0.131	0.111	0.164	14.121	12.052	1.178
4	Superstition Hills-02,1987	Poe Road (temp)	6.54	11.16	SS	0.475	0.286	0.164	51.181	31.109	1.660
5	Spitak-Armenia,1988	Gukasian	6.77	23.99	RO	0.200	0.174	0.116	21.639	18.879	1.150
6	Loma Prieta,1989	Coyote Lake Dam – SW Abut.	6.93	19.97	RO	0.132	0.280	0.089	7.160	15.239	0.470
7	Loma Prieta,1989	Fremont - Emerson Court	6.93	39.66	RO	0.192	0.099	0.068	10.442	5.412	1.927
8	Landers,1992	Mission Creek Fault	7.28	26.96	SS	0.097	0.132	0.078	5.235	7.059	0.734
9	Northridge-01,1994	LA - Pico & Sentous	6.69	27.82	R	0.103	0.186	0.064	11.199	20.229	0.553
10	Northridge-01,1994	LA - S. Vermont Ave	6.69	27.89	R	0.137	0.068	0.114	14.792	7.136	2.033
11	Northridge-01,1994	LA - Temple & Hope	6.69	28.82	R	0.124	0.165	0.097	13.378	17.875	0.750
12	Kobe-Japan,1995	Abeno	6.90	24.85	SS	0.149	0.231	0.110	16.092	25.006	0.644
13	Denali-Alaska,2002	Carlo (temp)	7.90	49.94	SS	0.081	0.084	0.071	8.719	9.085	0.971
14	San Simeon-CA,2003	Cambria - Hwy 1 Caltrans Bridge	6.52	6.97	R	0.179	0.126	0.085	9.736	6.796	1.425
15	Niigata-Japan,2004	FKS028	6.63	30.11	R	0.135	0.170	0.106	14.251	18.202	0.790
16	Niigata-Japan,2004	NIG023	6.63	25.33	R	0.405	0.248	0.081	44.049	26.983	1.631
17	Chuetsu-oki-Japan,2007	Nadachiku Joetsu City	6.80	35.79	R	0.119	0.155	0.051	12.841	16.858	0.769
18	Chuetsu-oki-Japan,2007	Tokamachi Chitosecho	6.80	25.35	R	0.201	0.251	0.062	21.158	27.282	0.802
19	Chuetsu-oki-Japan,2007	Kawaguchi	6.80	23.63	R	0.147	0.147	0.062	15.846	15.494	0.999
20	Chuetsu-oki-Japan,2007	NIG022	6.80	37.79	R	0.155	0.126	0.035	16.719	13.644	1.229
21	Iwate-Japan,2008	IWT010	6.90	16.26	R	0.226	0.289	0.204	24.403	31.345	0.781
22	Iwate-Japan,2008	Kami_ Miyagi Miyazaki City	6.90	25.15	R	0.117	0.156	0.072	12.628	16.871	0.748
23	Iwate-Japan,2008	Iwadeyama	6.90	20.77	R	0.269	0.354	0.178	29.220	38.187	0.759
24	Iwate-Japan,2008	Oomagari Hanazono-cho_ Daisen	6.90	46.32	R	0.093	0.127	0.054	10.109	13.670	0.735
25	Iwate-Japan,2008	Mizusawaku Interior O ganecho	6.90	7.82	R	0.361	0.257	0.188	37.630	27.556	1.403
26	Darfield-New Zealand,2010	DFHS	7.00	11.86	SS	0.275	0.333	0.374	14.940	18.122	0.826
27	Darfield-New Zealand,2010	DORC	7.00	29.96	SS	0.070	0.084	0.077	3.790	4.551	0.831
28	Darfield-New Zealand,2010	OXZ	7.00	30.63	SS	0.119	0.105	0.104	24.773	22.169	1.135
29	Darfield-New Zealand,2010	RKAC	7.00	13.37	SS	0.167	0.191	0.126	9.075	10.413	0.872
30	El Mayor-Mexico,2010	El Centro Array #4	7.20	35.08	SS	0.238	0.310	0.122	12.896	16.872	0.768

* Moment magnitude.

** Closest distance to fault rupture.

*** Fault mechanism, where R: reverse; SS: strike-slip; RO: reverse-oblique.

Table 3. Median (e^{μ}) and dispersion (σ) of the fitting lognormal distributions for the various groups and for the different limit states.

Id.	e^{μ}_{uplift} [g]	σ_{uplift} [g]	$e^{\mu}_{sliding}$ [g]	$\sigma_{sliding}$ [g]	$e^{\mu}_{collapse}$ [g]	$\sigma_{collapse}$ [g]
3-leg vessels						
1	0.1193	0.2067	0.1193	0.2067	0.3763	0.4736
2	0.1234	0.2475	0.1234	0.2475	0.4047	0.3053
3	0.1115	0.1762	0.1115	0.1762	0.3844	0.6608
4	0.1129	0.2020	0.1131	0.2054	0.3922	0.7588
5	0.1155	0.2373	0.1158	0.2359	0.4015	0.2906
6	0.1166	0.2518	0.1172	0.2541	0.3604	0.4459
7	0.1268	0.3090	0.1272	0.3080	0.4379	0.2473
8	0.1187	0.2083	0.1315	0.2184	0.4117	0.2533
9	0.1328	0.2489	0.1533	0.2499	0.4187	0.2502
10	0.1194	0.1817	0.1369	0.2208	0.4115	0.2195
11	0.1230	0.2290	0.1370	0.2201	0.3899	0.2623
12	0.1078	0.1429	0.1168	0.1776	0.4092	0.2132
13	0.1035	0.0571	0.1108	0.1229	0.4258	0.2613
14	0.1384	0.2259	0.1523	0.2212	0.4104	0.2519
15	0.1227	0.1808	0.1380	0.2185	0.4101	0.2165
16	0.1154	0.1662	0.1304	0.1758	0.4195	0.2185
17	0.1390	0.2550	0.1514	0.2434	0.4122	0.2364
18	0.1228	0.2006	0.1393	0.2280	0.4083	0.2097
19	0.1125	0.1609	0.1289	0.1897	0.4135	0.2313
20	0.1056	0.1140	0.1131	0.1644	0.4143	0.2550
4-leg vessels						
1	0.1529	0.3526	0.1585	0.3766	0.3808	0.5180
2	0.1572	0.4069	0.1669	0.4042	0.4290	0.2679
3	0.1525	0.2566	0.1702	0.2746	0.4294	0.2480
4	0.1363	0.2584	0.1601	0.2471	0.4232	0.2615
5	0.1676	0.2876	0.1963	0.2499	0.4698	0.2246
6	0.1418	0.2822	0.1709	0.2743	0.4625	0.2421
7	0.1487	0.2781	0.1770	0.2504	0.4466	0.2327
8	0.1331	0.2566	0.1591	0.2321	0.4353	0.2454
9	0.1404	0.2258	0.1625	0.2340	0.4373	0.2475
10	0.1401	0.2551	0.1644	0.2482	0.4599	0.2271
11	0.1404	0.2558	0.1652	0.2494	0.4775	0.2355
12	0.1212	0.1956	0.1374	0.2274	0.4473	0.2377
13	0.1046	0.0880	0.1292	0.1816	0.4319	0.2865
14	0.1205	0.1988	0.1374	0.2274	0.4413	0.2328
15	0.1113	0.1805	0.1227	0.1912	0.4453	0.2708
16	0.1089	0.1415	0.1209	0.1850	0.2094	0.2370
17	0.1059	0.1198	0.1106	0.1907	0.1036	0.2673
18	0.1544	0.4461	0.1572	0.4664	0.4061	0.3613
19	0.1481	0.2972	0.1570	0.3245	0.3772	0.2777
20	0.1268	0.2229	0.1507	0.2338	0.3285	0.2923
21	0.1284	0.2401	0.1349	0.2207	0.3746	0.2792
22	0.1429	0.2710	0.1628	0.2519	0.4135	0.2676
23	0.1421	0.2235	0.1638	0.2428	0.4232	0.2606
24	0.1178	0.1587	0.1392	0.2209	0.3703	0.2362
25	0.1381	0.2434	0.1631	0.2379	0.4637	0.2258
26	0.1177	0.2056	0.1441	0.2575	0.4288	0.1826
27	0.1229	0.2102	0.1475	0.2165	0.4468	0.2403
28	0.1138	0.1856	0.1381	0.2357	0.4365	0.2295

29	0.1050	0.1085	0.1304	0.2329	0.3318	0.2286
30	0.1168	0.1751	0.1228	0.1855	0.2738	0.3384
31	0.1574	0.3874	0.1775	0.3822	0.4491	0.2264
32	0.1253	0.1807	0.1466	0.2524	0.3837	0.2471
33	0.1660	0.3131	0.1920	0.2657	0.4765	0.2143
34	0.1195	0.1713	0.1378	0.2502	0.4180	0.2106
35	0.1687	0.3164	0.1974	0.3134	0.4894	0.2628
36	0.1476	0.2181	0.1745	0.2426	0.4662	0.2381
37	0.1345	0.2431	0.1559	0.2391	0.4404	0.2648
38	0.1238	0.2299	0.1385	0.2569	0.4352	0.2387
39	0.1165	0.1759	0.1319	0.2062	0.4151	0.2710
40	0.1102	0.1577	0.1321	0.1977	0.4229	0.2574
41	0.1150	0.1672	0.1266	0.2127	0.4394	0.2249
42	0.1179	0.1876	0.1332	0.2246	0.4468	0.1984
43	0.1301	0.2400	0.1651	0.2628	0.4608	0.2227
44	0.1264	0.2382	0.1418	0.2660	0.4620	0.2404
45	0.1221	0.2250	0.1384	0.2287	0.4491	0.2239
46	0.1173	0.2081	0.1290	0.2397	0.3306	0.2241
47	0.1152	0.2010	0.1296	0.2472	0.1812	0.2148
48	0.1142	0.2175	0.1208	0.2287	0.1253	0.2411
49	0.1082	0.1201	0.1109	0.1405	0.1109	0.1798
50	0.1065	0.1250	0.1102	0.1440	0.1158	0.2216
51	0.1009	0.0370	0.1070	0.1107	0.1110	0.1987
52	0.1027	0.0724	0.1062	0.1185	0.1089	0.2352
53	0.1049	0.0880	0.1116	0.1541	0.1215	0.2939
54	0.1051	0.0992	0.1114	0.1309	0.1236	0.2821
55	0.1369	0.3102	0.1369	0.3102	0.2056	0.6047
56	0.1273	0.2259	0.1497	0.2009	0.3912	0.2556
57	0.1181	0.1619	0.1366	0.1889	0.3844	0.2537
58	0.1141	0.1446	0.1397	0.1941	0.3534	0.2456
59	0.1160	0.1790	0.1323	0.2214	0.3767	0.2376
60	0.1150	0.2258	0.1268	0.2273	0.3572	0.2344
61	0.1497	0.2444	0.1772	0.2481	0.4543	0.2345
62	0.1359	0.2424	0.1686	0.2514	0.4525	0.2394
63	0.1292	0.2478	0.1543	0.2489	0.4407	0.1980
64	0.1215	0.2102	0.1388	0.2207	0.4354	0.2455
65	0.1206	0.1957	0.1389	0.2127	0.4188	0.1951
66	0.1132	0.1869	0.1340	0.2324	0.3897	0.2615
67	0.1104	0.1491	0.1298	0.1995	0.3976	0.2556
68	0.1116	0.1341	0.1332	0.2143	0.3852	0.2887
69	0.1568	0.3189	0.1932	0.2647	0.4879	0.2136
70	0.1348	0.2239	0.1562	0.2712	0.4506	0.1910
71	0.1178	0.1915	0.1335	0.2269	0.4332	0.2511
72	0.1108	0.1442	0.1332	0.2050	0.4273	0.2645
73	0.1059	0.1139	0.1063	0.1133	0.1248	0.3254
74	0.1070	0.1080	0.1132	0.1737	0.1270	0.2783
75	0.1122	0.1447	0.1206	0.1952	0.1304	0.2648
76	0.1077	0.1290	0.1419	0.2069	0.3981	0.2574
77	0.1101	0.1615	0.1341	0.2194	0.4293	0.2123
78	0.1052	0.1389	0.1340	0.1985	0.4252	0.3163
79	0.1097	0.1471	0.1255	0.2188	0.4221	0.2603
80	0.1043	0.0802	0.1332	0.2257	0.1270	0.2451
81	0.1126	0.1828	0.1266	0.2062	0.4348	0.2063
82	0.1053	0.0861	0.1282	0.2081	0.4173	0.2753
83	0.1033	0.0776	0.1410	0.2507	0.1434	0.2601
84	0.1111	0.1609	0.1249	0.1985	0.4509	0.2719
85	0.1054	0.1064	0.1248	0.2011	0.1901	0.2563
86	0.1066	0.1113	0.1308	0.2072	0.1290	0.2510

87	0.1036	0.0815	0.1224	0.2109	0.1252	0.2629
88	0.1034	0.0740	0.1162	0.1980	0.1138	0.2680
89	0.1062	0.1215	0.1219	0.1987	0.1547	0.2255
90	0.1033	0.0810	0.1199	0.1839	0.1524	0.2629
91	0.1094	0.1281	0.1300	0.2441	0.1709	0.2962
92	0.1088	0.1433	0.1107	0.1466	0.1273	0.2814
93	0.1088	0.1412	0.1282	0.1982	0.3896	0.2611
94	0.1525	0.2448	0.1806	0.2433	0.4788	0.2315
95	0.1318	0.2399	0.1535	0.2693	0.4424	0.2554
96	0.1209	0.2101	0.1335	0.1799	0.4358	0.2166
97	0.1125	0.1732	0.1320	0.2103	0.2772	0.2150
98	0.1185	0.2095	0.1419	0.2447	0.4328	0.2613
99	0.1126	0.2052	0.1287	0.2370	0.2369	0.2362
100	0.1059	0.0907	0.1104	0.1061	0.1196	0.1658
101	0.1127	0.1940	0.1156	0.2107	0.1190	0.2324
102	0.1055	0.0969	0.1055	0.0969	0.1128	0.1996
103	0.1039	0.0907	0.1174	0.2169	0.1224	0.3134
104	0.1046	0.0882	0.1157	0.1659	0.1226	0.2709
105	0.1088	0.1432	0.1116	0.1538	0.1126	0.1883
106	0.1034	0.0689	0.1056	0.0821	0.1118	0.1835
107	0.1048	0.0975	0.1134	0.1890	0.1197	0.2570
108	0.1028	0.0632	0.1133	0.1518	0.1209	0.2678
109	0.1040	0.0819	0.1180	0.1672	0.1305	0.2883
110	0.1479	0.2326	0.1742	0.2713	0.4092	0.2229
5-leg vessels						
1	0.1623	0.3044	0.1987	0.2610	0.5172	0.2340
2	0.1356	0.2229	0.1733	0.2175	0.4848	0.2733
3	0.1170	0.1797	0.1582	0.2370	0.4576	0.2560
4	0.1475	0.2615	0.1839	0.2596	0.5155	0.2414
5	0.1326	0.2223	0.1694	0.2317	0.4982	0.2596
6	0.1249	0.2294	0.1488	0.2379	0.4772	0.2280
7	0.1073	0.1110	0.1447	0.2139	0.4760	0.2638
8	0.1613	0.2982	0.2048	0.2673	0.5326	0.2554
9	0.1453	0.2865	0.1882	0.2555	0.5179	0.2333
10	0.1261	0.2501	0.1601	0.2851	0.5034	0.2350

Table 4. Regression parameters of Eq.(9) defining the response surfaces of fitting lognormal distribution median (e^{μ}) for the various groups and for the different limit states.

	a_0 [g]	a_1 [g]	a_2 [g]	a_3 [g T^{-1}]	a_4 [g T^{-2}]	R_{adj}^2
			3-leg vessels			
e^{μ}_{uplift}	0.32527	-0.18535	0.04079	0.00031	-0.00003	0.778
$e^{\mu}_{sliding}$	0.40985	-0.27092	0.06265	0.00295	-0.00013	0.851
$e^{\mu}_{collapse}$	0.71677	-0.31708	0.07722	0.00246	-0.00008	0.750
			4-leg vessels			
e^{μ}_{uplift}	0.21688	-0.05682	0.00895	-0.00100	0.00001	0.895
$e^{\mu}_{sliding}$	0.27485	-0.09162	0.01674	-0.00109	0.00001	0.868
$e^{\mu}_{collapse}$	0.72728	-0.19308	0.03058	-0.00578	0.00002	0.866
			5-leg vessels			
e^{μ}_{uplift}	0.29391	-0.08489	0.01386	-0.00710	0.00021	0.929
$e^{\mu}_{sliding}$	0.38744	-0.18066	0.04023	-0.00210	-0.00001	0.990
$e^{\mu}_{collapse}$	0.70517	-0.11609	0.00941	-0.00934	0.00047	0.940

Table 5. Regression parameters of Eq.(10) defining the response surfaces of fitting lognormal distribution dispersion (σ) for the various groups and for the different limit states.

	b_0 [g]	b_1 [g mm^{-1}]	b_2 [g]	b_3 [g T^{-1}]	b_4 [g mm T^{-1}]	R_{adj}^2
			3-leg vessels			
σ_{uplift}	0.54665	0.00001	-0.15454	0.00299	-35.00969	0.908
$\sigma_{sliding}$	0.45100	0.00009	-0.12877	0.00573	-73.40685	0.863
$\sigma_{collapse}$	0.84283	-0.00096	0.09597	-0.00859	367.61942	0.739
			4-leg vessels			
σ_{uplift}	0.64083	-0.00005	-0.13171	0.00384	-27.61005	0.848
$\sigma_{sliding}$	0.44914	0.00001	-0.07004	0.00239	-32.96025	0.760
$\sigma_{collapse}$	0.44629	-0.00015	0.00508	0.00115	25.75410	0.731
			5-leg vessels			
σ_{uplift}	2.25920	-0.00114	-0.34152	0.02564	197.56826	0.884
$\sigma_{sliding}$	-0.09159	0.00050	-0.14399	0.01314	-173.75168	0.752
$\sigma_{collapse}$	1.53206	-0.00127	0.09979	-0.00985	379.51286	0.698